Revised Response to Reviewer #2 Comment

Dear Prof. Knopf,

We thank you for catching the error in our discussion of the aspiration efficiency and the potential impact of non-isokinetic sampling. We provide below a revised response to the reviewer comment (with more explicit calculations). We have also added a very short discussion to the main text (given below). Although our initial presentation of the aspiration efficiency was in error, we note that our conclusion was correct, namely that the differences in sampling between instrument groups from the manifold and the lack of explicit isokinetic sampling did not lead to the instrument groups sampling different particle populations.

Sara Forestieri and Chris Cappa

Authors' Comment: Page4, Line 24. I wonder if the flow was split isokinetically (equal face velocities) between instruments sampling from MART as that could affect sampled particle sizes of individual instruments. The authors mentioned laminar conditions, but laminar conditions limit particle losses to tubing walls while isokinetic split maintains the same particle population into each sampling line.

Revised Response: The reviewer raises an important question about the comparability of the measurements between instruments due to differences in sampling. During these experiments, flow was not split isokinetically. The particle-laden air from the MART was sampled into a manifold. The individual instruments sampled from this manifold from one of a many "ports". The flow rate to each instrument (or group of instruments), and thus the flow from each port, varied. For example, for Group 1 the CRD + SEMS sampled a much higher flow rate (3 LPM) than the AMS and ATOFMS (~ 0.7 to 1 LPM) from the manifold. Therefore, it is possible that the instruments sampled particle populations with different sizes. It is difficult to estimate differential losses between the different ports due to flow rate differences in this configuration. The equations describing aspiration efficiency for isoaxial sampling from an air stream typically have a form similar to (Kulkarni et al., 2011):

$$\eta_{asp} = 1 + \left[\frac{U_0}{U} - 1\right]\left[1 - \frac{1}{1 + kStk}\right]$$

where η_{asp} is the aspiration efficiency, U_0 is the ambient gas stream velocity, U is the sampling velocity, k = 2+0.67(U/U_0) and Stk is the Stokes number, where

$$Stk = \frac{\tau_p \cdot U_0}{D_{tubing}}$$

with τ_p the (size-dependent) particle relaxation time and D_{tubing} the diameter of the sampling tube. For the manifold system here, the effective ambient gas stream velocity in the sampling manifold was 0.08 m/min, while the CRD and the AMS had sampling velocities of 26.5 and 8.8 m/min, respectively and the inlet diameters on the manifold were ~0.012 meters for both the CRD and AMS. For particles < 1 µm (particle relaxation times ~10^{-6} s), the aspiration efficiencies were calculated to be nearly 100% for both systems. For particles > 10 µm (particle relaxation time ~10^{-4} s) , the aspiration efficiencies were 88% and 96% for the CRD and AMS, respectively; such large particles make up a negligible fraction of the total particle populations sampled here. Thus, the particle population will not be strongly influenced by the non-isokinetic sampling conditions and the lack of explicit isokinetic sampling did not have a substantial impact on the measurements here. We have added the following text to the manuscript associated with this issue:

"The flowrates to each instrument (or group of instruments) from ports in the manifold differed (e.g. 1 lpm to the AMS versus 3 lpm to the CRD + SEMS). Although the airstreams were not split iso-kinetically, the aspiration efficiency was calculated to be near 100% for the size range of particles sampled here (Kulkarni et al., 2011). Thus, the different instrument groups sampled similar particle populations from the manifold."

References

Kulkarni, P., Baron, P. A., and Willeke, K.: Aerosol measurement: principles, techniques, and applications, John Wiley & Sons, 2011.

Linking variations in sea spray aerosol particle hygroscopicity to composition during two microcosm experiments

Sara D. Forestieri[1], Gavin C. Cornwell[2], Taylor M. Helgestad[1], Kathryn A. Moore[2], Christopher Lee[2], Gordon A. Novak[3], Camille M. Sultana[2], Xiaofei Wang[2], Timothy H. Bertram[2,3], Kimberly A. Prather[2,4], Christopher D. Cappa[1,*]

[1]Department of Civil and Environmental Engineering, University of California, Davis, CA 95616
[2] Department of Chemistry and Biochemistry, University of California, San Diego, La Jolla, CA 92093
[3] Department of Chemistry, University of Wisconsin, Madison, WI 53706
[4] Scripps Institution of Oceanography, 9500 Gilman Drive, La Jolla, CA 92093

[*] Correspondence to: E-mail: cdcappa@ucdavis.edu

Abstract. The extent to which water uptake influences the light scattering ability of marine sea spray aerosol (SSA) particles depends critically on SSA chemical composition. The organic fraction of SSA can increase during phytoplankton blooms, decreasing the salt content and therefore the hygroscopicity of the particles. In this study, subsaturated hygroscopic growth factors at 85% relative humidity (*GF*(85%)) of predominately submicron SSA particles were quantified during two induced phytoplankton blooms in marine aerosol reference tanks (MARTs). One MART was illuminated with fluorescent lights and the other was illuminated with sunlight, referred to as the "indoor" and "outdoor" MARTs, respectively. Optically weighted *GF*(85%) values for SSA particles were derived from measurements of light scattering and particle size distributions. The mean optically weighted SSA diameters were 530 nm and 570 nm for the indoor and outdoor MARTs, respectively. The *GF*(85%) measurements were made concurrently with online particle composition measurements, including bulk composition (using an Aerodyne high-resolution aerosol mass spectrometer) and single particle (using an aerosol time-of-flight mass spectrometer) measurement, and a variety of water-composition measurements. During both microcosm experiments, the observed optically-weighted *GF*(85%) values were depressed substantially relative to pure, inorganic sea salt, by 5 to 15%. There was also a time lag between *GF*(85%) depression and the peak chlorophyll-a (Chl-a) concentrations, by either one (indoor MART) and three-to-six (outdoor MART) days. The fraction of organic matter in the SSA particles

generally increased after the Chl-a peaked, also with a time lag, and ranged from about 0.25 to 0.5 by volume. The observed depression in the *GF*(85%) values (relative to pure sea salt) is consistent with the large observed volume fractions of non-refractory organic matter (NR-OM) comprising the SSA. The *GF*(85%) values exhibited a reasonable negative correlation with the SSA NR-OM volume fractions after the peak of the blooms (i.e. Chl-a maxima), i.e. the *GF*(85%) values generally decreased when the NR-OM volume fractions increased. The *GF*(85%) versus NR-OM volume fraction relationship was interpreted using the Zdanovskii-Stokes-Robinson (ZSR) mixing rule, and used to estimate the *GF*(85%) of the organic matter in the nascent SSA. The estimated pure NR-OM *GF*(85%) values were 1.16 ± 0.09 and 1.23 ±0.10 for the indoor and outdoor MARTS, respectively. These measurements demonstrate a clear relationship between SSA particle composition and the sensitivity of light scattering to variations in relative humidity. The implications of these observations to the direct climate effects of SSA particles are discussed.

1 Introduction

Aerosols impact climate directly by scattering and absorbing solar radiation and indirectly by modifying cloud properties (IPCC, 2013). Sea spray aerosol (SSA) particles are a major source of natural aerosols to the atmosphere and dominate the pre-industrial clear-sky direct radiative effects over the ocean (Haywood et al., 1999). Breaking waves in the ocean entrain air into seawater leading to the formation of bubbles, which burst at the ocean's surface, producing SSA particles (Lewis and Schwartz, 2004). The climate impacts of SSA particles depend critically on their composition, shape, and size (Carslaw et al., 2013; Pilinis et al., 1995). Given typical size distributions for particles in the marine boundary layer, both the submicron (300-1000 nm) and supermicron (~1-5 μm) size ranges contribute to light scattering, with the relative contributions varying depending on location and conditions (Kleefeld et al., 2002). Under humidified conditions, the size of SSA particles is modified through water uptake and loss, which are a strong function of chemical composition (Saxena et al., 1995). The overall mass of SSA particles is dominated by sodium chloride and other inorganic ions, but organic compounds can also contribute substantially to the total mass, especially in the submicron size regime (Facchini et al., 2008; Keene et al., 2007; O'Dowd et al., 2004). Larger organic matter-to-salt ratios occur in the submicron mode through the formation of film drops, since surface-active organics can become enriched in the thin film prior to bubble bursting (Skop et al., 1994; Stefan and Szeri, 1999; Tseng et al., 1992), but it has also been shown that supermicron particles can also contain organic and biological markers (Quinn et al., 2015). Since organic compounds are universally less hygroscopic than inorganic sea salt (Petters and Kreidenweis, 2007), their transfer to SSA will lead to less water uptake and, thus, less scattering than in the case of pure inorganic sea salt particles of the same size.

Previous studies have linked the suppression of water uptake of ambient SSA particles to increasing fractions of marine-derived organic matter in the ambient atmosphere (Vaishya et al., 2013; Ovadnevaite et al., 2011; Lawler et al., 2014; Hegg et al., 2008; Zhang et al., 2014). Phytoplankton blooms lead to chemical changes in seawater and serve as a source of particulate and dissolved organic carbon (DOC) to the system, which is then processed by other micro-organisms as part of the microbial loop (Pomeroy et al., 2007). These chemical and biological changes in the seawater can impact SSA particle composition (Prather et al., 2013; Lee et al., 2015; O'Dowd et al., 2004). The organic fraction of SSA particles has been correlated to metrics for high biological activity, such as chlorophyll-a, in some studies (O'Dowd et al., 2004; Facchini et al.,

2008), but not others (Quinn et al., 2014). Some lab studies have observed small depressions in water uptake by SSA particles produced from natural seawater relative to synthetic, inorganic seawater (Sellegri et al., 2008; Modini et al., 2010; Fuentes et al., 2011; Park et al., 2014). However, all of these studies have focused on particles smaller than ~150 nm, for which variations in composition have bigger impacts on cloud condensation nuclei concentrations (Dusek et al., 2006; Farmer et al., 2015). Substantially less is understood about the connections between seawater composition and the water uptake properties of the larger submicron particles that contribute more to light scattering. The connection between biological and chemical characteristics of seawater and the resulting SSA particle composition, and consequently hygroscopicity, has therefore not been fully established.

To better understand the connection between SSA particle composition and water uptake as it relates to light scattering in particular, two microcosm experiments were conducted in July 2014 as part of IMPACTS (Investigation into Marine Particle Chemistry and Transfer Science). Through the addition of light and nutrients, phytoplankton blooms were induced in natural seawater. Marine aerosol reference tanks (MARTs) were used to produce SSA particles via intermittent plunging of a sheet of water, which reproduces the bubble size distribution of whitecaps in the ocean (Lee et al., 2015; Stokes et al., 2013). Studying the SSA particles produced during these microcosm studies can provide insights into the linkage between hygroscopicity of nascent SSA particles and ocean biology in an environment that is isolated from anthropogenic influence or background particles. The simultaneous measurement of submicron SSA particle water uptake and of particle composition here demonstrate that variations in seawater biology and composition influence water uptake by SSA particles.

2 Methods

2.1 MART Description and Operation

Two separate experiments were conducted during July 2014 utilizing MARTs. Detailed information on the performance and operation of MARTs can be found in Stokes et al. (2013) and only a brief description will be provided here. SSA particles were generated in an enclosed 210 L acrylic tank via an intermittent plunging sheet of water operated on a computer-controlled 4-seconds-on, 4-seconds-off cycle to allow for surface foam evolution and dissipation close to what

would be observed for natural whitecaps in the ocean. The plunging cycle creates a constant, reproducible concentration of nascent SSA particles in the 90 L headspace, with SSA particle size distributions produced in the MARTs generally consistent with those observed for SSA particles from lab generated breaking waves (Stokes et al., 2013). SSA particles sampled from the MARTs are primary, since the average residence time in the MARTs is much shorter than the time scale required for secondary processing of SSA particles (e.g. heterogeneous gas-phase reactions) (Lee et al., 2015). SSA particles from the headspace were sampled periodically each day by instruments that characterized SSA particle size distributions, composition, and optical and hygroscopic properties. SSA were sampled from the MART headspace and transported through an approximately 2 m long line of 3/8 in. conductive tubing into a laminar flow manifold from which the instruments sampled. The flowrates to each instrument (or group of instruments) from ports in the manifold differed (e.g. 1 lpm to the AMS versus 3 lpm to the CRD + SEMS). Although the airstreams were not split iso-kinetically, the aspiration efficiency was calculated to be near 100% for the size range of particles sampled here (Kulkarni et al., 2011). Thus, the different instrument groups sampled similar particle populations from the manifold. Due to the limited headspace volume and flow restrictions, not all instruments in this study could sample simultaneously. During individual sampling periods, only a subset of the full instrument suite sampled from the MARTs. The flow rate of zero air going into the MART and the flow being pulled from the MART by the instruments, as well as sampling times for each group of instruments, are provided in Table 1. The flow into the MART was always 1 LPM greater than the combined instrument pull to ensure positive pressure in the headspace, which eliminated possibility of sampling of room air. The shape of the measured particle size distributions were relatively independent of flow rate for the range of flow rates considered while sampling from the MARTs, although the residence time of individual particles decreases as the flow rate increases (Stokes et al., 2013). The air pushed into the MART was produced by a zero air generator (Sabio Instruments, Model 1001), with air flow controlled by a mass flow controller. The excess flow was released through a vent on the MART. The different flow rates through the MART and through the sample tubing for each sampling configuration led to some differences in the size distribution sampled by the downstream instrumentation.

The procedure for inducing phytoplankton blooms inside of the MARTs will be briefly described here; further general details can be found in Lee et al. (2015). The MARTs were filled

with ~120 L of seawater each collected from the SIO pier in La Jolla, California, USA (32°51´56.8"N: 117° 15´38.48"W). Debris and zooplankton were filtered out of the seawater with 50 μm mesh. Phytoplankton growth was induced by exposure to artificial or natural light and the addition of growth media, which is described further in Lee et al. (2015). The two independent MART experiments will be referred to according to the MART location during the growth phase, either "indoor" or "outdoor". The indoor MART was illuminated using 5700 K full spectrum lights, while the outdoor MART was illuminated with sunlight. A key difference between these two experiments is the intensity of the photosynthetically active radiation (PAR) during growth. The PAR was much greater for the outdoor MART compared to the indoor MART (PAR~1000-1500 μE m^{-2} s^{-1} (Bouvet et al., 2002) versus ~70 μE m^{-2} s^{-1}), which likely resulted in a much larger peak Chl-a concentration for the outdoor MART, 51 μg L^{-1} (outdoor) versus 10 μg L^{-1} (indoor). An additional difference between the two microcosms was that the seawater was collected on different days, 8 July for the indoor MART and 19 July for the outdoor MART. The conditions of the seawater at time of collection are detailed in Table 2.

On 9 July, particles from the indoor MART were sampled immediately following nutrient addition. Further sampling was delayed until Chlorophyll-a (Chl-a) concentrations exceeded approximately 12 μg L^{-1}, which occurred seven days after nutrient addition. (The same seawater as used in the indoor MART was added to a separate MART and sampled immediately after collection and before nutrient addition. However, the resulting particle size distribution from this MART differed substantially from those measured from the indoor MART, with a much greater contribution of large particles. Thus, the measurements from this separate MART are not directly comparable to the measurements from the indoor MART and are not considered further.) The outdoor MART was only sampled after Chl-a concentrations exceeded approximately 12 μg L^{-1}, which occurred three days after nutrient addition. This delay in sampling from when the water and nutrients were first added to the MARTs is necessary because the plunging process can lead to lysis of the phytoplankton cells during this vulnerable growth period, which will inhibit phytoplankton growth (Lee et al., 2015). Ultimately, SSA from the initially collected water from the indoor MART was sampled on 9 July, and subsequent sampling commenced periodically from 19 July through 31 July, i.e. beginning 11 days after the water was collected. Sampling from the outdoor MART did not commence until 22 July, continuing through 1 August. During the growth period and the off-sampling periods, air was gently bubbled through the tank to provide aeration.

Sampling from the MARTs was performed daily once the threshold chlorophyll-a concentrations were reached.

2.2 Instrumentation

A variety of online and offline measurements were made to characterize water composition and particles generated within the MARTs. A general sampling schematic is shown in Figure 1 and a list of the instrumentation used is given in Table 1. As only a limited number of instruments were able to sample concurrently from the MART due to flow limitations, the individual sampling configurations (i.e. groupings of instruments sampling at the same time) are indicated; three specific instrument groupings are considered. The sampling times of each group relative to Group 1 are listed in Table 1 and a more detailed schematic of Group 1 optical and sizing measurements is provided in Figure S1. (The specific timing was dictated by the broader goals of IMPACTS.) A general description of the key instrumentation used as part of this study is provided below. Group 1 sampled for 1.5 h, group 2 sampled for 2 h, and Group 3 for sampled 1 h each day that sampling was conducted.

2.2.1 Online particle measurements

Size distributions for dried particles (RH < 20%) were measured with a scanning electrical mobility sizer (SEMS; BMI; model 2002), and an aerodynamic particle sizer (APS; TSI Inc.; Model 3321). The SEMS combines a differential mobility analyzer (DMA) and a mixing condensation particle counter (MCPC) to characterize particles according to their mobility diameter ($d_{p,m}$). The APS characterizes particles according to their aerodynamic diameter ($d_{p,a}$). The SEMS characterized particles over the range 10 nm < $d_{p,m}$ < 1900 nm and the APS over the range 0.7 μm < $d_{p,a}$ < 20 μm. The SEMS size distributions were corrected for the influence of multiply charged particles using software provided by the manufacturers. No diffusion correction was performed, which has negligible influence on this study because the smallest particles (<100 nm), which are sensitive to diffusion corrections, contribute negligibly to the observed scattering. The APS had a time resolution of 1 minute, while the SEMS had a time resolution of 5 minutes and the APS distributions were accordingly averaged to 5 minutes to facilitate generation of a merged size distribution. The SEMS and APS distributions were merged using the SEMS

distribution up to 1 μm and the ($d_{p,m}$ equivalent) APS distribution at larger diameters. The APS $d_{p,a}$ values were converted to mobility equivalent values assuming a particle density of 1.8 g cm^{-3}.

The hygroscopicity of the SSA particles was characterized through simultaneous measurement of light extinction coefficients (b_{ext}) for particles that were either dried to RH < 20% ("dry") or humidified to RH ~85% ("wet") using the UC Davis cavity ringdown spectrometer (CRD) (Langridge et al., 2011; Cappa et al., 2012). Light absorption by the SSA particles was negligible, and thus extinction is equal to scattering, i.e. $b_{ext} = b_{sca}$. The dry particle measurements were made at wavelengths of 532 nm and 405 nm, while the wet particle measurements were made only at 532 nm. It should be noted that the humidified particle stream was generated without first drying the particles, and thus it is unlikely that the sampled particles had effloresced. Humidification was achieved by passing the particles through a Nafion humidifier (Permapure, MD-110-12) while drying was achieved by passing the particles through a diffusion denuder filled with Drierite. Both the humidifier and drier were oriented vertically to prevent differential losses due to sedimentation, which could bias the measurements. The fundamental performance of the CRD method for wet particles is the same for dry particles, but variations and uncertainty in the relative humidity (RH) contribute to the uncertainty in the measured b_{ext}. The RH for the humidified channel varied between 80-87% due to challenges in maintaining a constant temperature in the open-air Scripps Hydraulics Lab; these variations are accounted for in the analysis as described below. The RH of the air was measured directly in the CRD cells using RH probes (Vaisala, HMP50) that were calibrated against saturated salt solutions. The wet (high RH) and dry (low RH) particle measurements are combined to provide a characterization of the extent of water uptake at a given RH, which causes particles to grow through the parameter *f*(RH), where:

$$f(RH) = \frac{b_{ext}(RH_{high})}{b_{ext}(RH_{low})} = \frac{b_{sca}(RH_{high})}{b_{sca}(RH_{low})} \quad (1).$$

The parameter *f*(RH) is RH-specific, and is most appropriate when RH_{low} is sufficiently low that there is little, if any particle-phase water. The accuracy of the *f*(RH) measurements, as well as the conversion to equivalent growth factors (*GF*, Section 2.2.3), were tested through measurements

made using sodium chloride and ammonium sulfate particles that were generated using an atomizer.

The CRD (and SEMS) alternated between sampling behind a $PM_{2.5}$ cyclone and with no explicit size cut (referred to as PM_{all}) every ten minutes to try and determine f(RH) and GF values separately for smaller and larger particles. Note that particles were sampled through the $PM_{2.5}$ cyclone prior to being dried (RH~70%) and thus the effective size cut for the subsequently dried particles is somewhat less than 2.5 μm, depending on the exact water content of the particles at 70% RH. Since the measured size distributions indicate minimal contributions from particles with $d_{p,a}$ > 2.5 μm, the $PM_{2.5}$ and PM_{all} measurements will generally be considered together.

An aerosol time of flight mass spectrometer (ATOFMS) (Gard et al., 1998; Pratt et al., 2009) was used to characterize the composition of individual dried SSA particles with vacuum aerodynamic diameters (d_{va}) from ~300 nm to 3 μm, with the highest transmission and sampling of particles with d_{va} ~1-2 μm (Wang et al., 2015). The ATOFMS single particle spectra have been analyzed using a statistical clustering algorithm (ART-2a) that groups particles with similar spectra together (Zhao et al., 2008). Six particle mass spectra categories were generated and are described as: sea salt (SS), salt mixed with organic carbon (SSOC), predominately OC containing (OC), containing a large Fe peak (Fe) and containing a large Mg Peak (Mg) (Lee et al., 2015; Sultana et al., In Prep.; Wang et al., 2015). A campaign-average spectrum for each category is shown in Figure S2. The combination of the aerodynamic lens transmission and the input particle size distribution determines the particular weighting of the average fractions of the ATOFMS particle types (see Figure S3); in this study, the results are for the sampling-weighted average, which corresponds approximately to a sampling-weighted average d_{va} = 1.5 μm.

An Aerodyne high resolution time-of-flight aerosol mass spectrometer (HR-ToF-AMS, henceforth AMS) quantified mass concentrations of non-refractory (NR) components of dried SSA particles, in particular NR organic matter (NR-OM) but also other non-refractory (NR-PM) components (Canagaratna et al., 2007). NR-PM species are defined as those that volatilize at ~600 °C on a time scale of a few seconds under vacuum (10^{-4} torr) conditions. No cyclone was used in front of the AMS, and thus the size range of sampled SSA particles was determined by the size-dependent transmission of the aerodynamic lens, which nominally allowed for quantitative sampling of particles with d_{va} between 90 nm and 700 nm (50% cut points at ~40 nm and ~1

micron), although some fraction of even larger particles were characterized (Wang et al., 2015). The AMS data were analyzed using the SQUIRREL toolkit. The high resolution mass spectra were analyzed using the PIKA toolkit to determine O/C atomic ratios for the NR-OM components. The NR-OM fraction of total sampled PM was estimated by normalizing the NR-OM mass concentrations by PM_1 concentrations determined from integration of the SEMS particle size distributions using an assumed density of 1.8 g cm^{-3}. Since a d_{va} of 1 μm corresponds approximately to a $d_{p,m}$ = 560 nm, the use of the SEMS size distribution is appropriate and the derived NR-OM fractions can be considered reflective of the submicron SSA composition. It is important to note that while the temporal trends of the AMS NR-OM/PM_1 fractions are likely reflective of the general behavior, the absolute values are more difficult to quantify because NR-OM associated with particles containing high sea salt fractions may not be vaporized efficiently by the AMS due to the refractory nature of sea salt (Frossard et al., 2014) and to the susceptibility of SSA particles to particle "bounce" in the AMS. Consequently, the SSA particles, including the NR-OM component, are detected with a collection efficiency (*CE*) lower than unity (Frossard et al., 2014). One previous study (Ovadnevaite et al., 2012) determined the *CE* value for organic-free sea salt sampled when RH < 70% is approximately 0.25. However, they also note that the *CE* is potentially instrument dependent, and further may not be applicable to the organic fraction in sea spray particles due to differences in ionization efficiency (which is a component of the overall *CE*) (Ovadnevaite et al., 2012). It is also possible that the *CE* differs between particles that have differing relative amounts of OM and sea salt. Despite such uncertainties in quantification of NR-OM by the AMS for sea spray particles, the NR-OM mass concentrations for the sampled SSA particles were determined in this study assuming *CE* = 0.25. The measured NR-OM mass concentrations were used to calculate NR-OM volume concentrations assuming a density (ρ) of 1.0 g/cm^3. A value of 1.0 g/cm^3 for ρ_{OM} is consistent with that of fatty acids (ρ < 1 g/cm^3), which are a significant fraction of marine-derived OM (Cochran et al., 2016; Mochida et al., 2002). However, this value serves as a lower bound for ρ_{OM} because OM with higher densities, such as sugars (ρ ~ 1.7 g/cm^3), have also been observed in SSA (Quinn et al., 2015). The NR-OM volume fractions of SSA (ε_{org}) were calculated as the ratio between the observed NR-OM volume concentrations and the integrated total particle volume concentrations from the size distribution measurements. Given the use of a lower-limit value for ρ_{OM} the ε_{org} are likely upper limits (not accounting for uncertainty in the assumed *CE*).

2.2.2 Optical closure methods

The *f*(RH) values measured using the CRD instrument have been used to determine optically-weighted physical growth factors (*GF*s). For particles of a given size, the *GF* is defined as:

$$GF(RH) = \frac{d_{\mathrm{p}}(\mathrm{RH_{high}})}{d_{\mathrm{p}}(\mathrm{RH_{low}})} \quad (2)$$

where d_{p} is the geometric particle diameter, which is equivalent to $d_{\mathrm{p,m}}$ for spherical particles. For clarity, in this work the optically-weighted *GF* will be indicated simply as *GF*, while size-specific *GF* values will be indicated as GF_{x}. SSA particle composition can vary with size (e.g. O'Dowd et al., 2004), and thus GF_{x} values may vary with size. The optically-weighted *GF* averages across size-dependent variations in composition and GF_{x} to focus on the chemical changes that most influence water uptake by the particles that most contribute to light scattering. Unlike *f*(RH), GF_{x} values are independent of the dry particle size (above about 100 nm diameter) for particles of a given composition. Thus, variations in the optically-weighted *GF* values are driven only by variations in particle composition, specifically variations in the average composition of particles in the size range over which the optical measurements are most sensitive. For the measurements here, the sensitive size range is between about 400 nm and 800 nm, with particles below 200 nm contributing almost zero to the observed scattering (see Section 3.1 below).

The observed *f*(RH) values are converted to *GF*(RH) values via optical closure. The optical closure technique uses spherical particle Mie theory calculations and the measured size distributions and *f*(RH) values to derive equivalent *GF*(RH) values. This methodology is described in detail in Zhang et al. (2014). In brief, the dry scattering is first calculated from the measured dry particle size distribution assuming a refractive index of 1.55 (the refractive index for NaCl), as:

$$b_{sca} = \int \sigma_{sca}(d_{p,m}) \cdot \frac{dN}{d\log d_{p,m}} d\log d_{p,m} \quad (3)$$

where σ_{sca} is the size-dependent scattering cross section and $dN/d\log d_{p,m}$ is the number-weighted size distribution. Then, each diameter for the dry distribution is multiplied by a trial value for *GF*(RH), the refractive index of the particles is adjusted to account for the resulting volume fraction of water, and the scattering by the resulting "wet" distribution is calculated, from which a theoretical *f*(RH) value is determined. The calculated *f*(RH) is compared to the observed *f*(RH), and if the two do not agree to within 0.01 the trial *GF*(RH) is increased until closure is obtained. It is assumed that the growth factors are size independent, namely that $GF_x = GF$ for all d_p. Thus, this method retrieves an effective, optically-weighted *GF* value that explains the observed influence of water uptake on light scattering for the sampled size distribution. An alternative approach was considered in which the GF_x were assumed to vary with size, specifically as $GF_x = 2.1 - b\ (\log(1.8\ \mu m) - \log(d_{p,m}))$, and where the value of *b* was allowed to vary during the optical closure, with the condition that $GF_x \geq 0$. (This expression assumes that particles with $d_{p,m} = 1.8$ have a $GF_x = 2.1$, i.e. that of NaCl. The GF_x decrease as size decreases.) The derived *b* values exhibit a similar temporal dependence as the derived optically-weighted *GF* values. The general conclusions reached in this study are therefore independent of the assumptions made regarding the size-dependent behavior of GF_x. Thus, rather than introducing an uncertain functional form, the simpler assumption (namely, size-independent GF_x values) is used here.

As the RH of the humidified channel was not perfectly constant during measurements, the derived individual *GF*(RH) values have been adjusted to 85% by using Equation 4:

$$\frac{RH}{\exp\left(\frac{A}{d_d * GF(RH)}\right)} = \frac{GF(RH)^3 - 1}{GF(RH)^3 - (1-\kappa)} \quad (4)$$

where *A* is a constant, RH is relative humidity, d_d is the dry particle diameter and κ is the effective hygroscopicity parameter, which is assumed to be RH-independent (Petters and Kreidenweis, 2007). Here, the d_d values used are the optically-weighted median diameters, which are calculated by integrating the concentration-weighted size-dependent cross-sections ($\sigma_{sca}(d_p)$). *GF*(85%) values were determined by first calculating κ based on the measured *GF*(RH) and then recalculating the *GF* at 85% RH.

The accuracy of this optical closure method, as well as of the initial *f*(RH) measurements, was assessed by comparing the *GF*(85%) values determined for polydisperse distributions of NaCl and $(NH_4)_2SO_4$ test particles, for which *GF*(85%) values are known. The measured *GF*(85%) for NaCl was 2.09 +/- 0.03 and for $(NH_4)_2SO_4$ was 1.59 +/- 0.05, which compare very well with literature values of ~2.1 for NaCl (Cruz and Pandis, 2000; Laskina et al., 2015; Hansson et al., 1998) for particle sizes ranging from 100 nm to 300 nm and ~1.55 for ammonium sulfate (Laskina et al., 2015; Wise et al., 2003) for 100 nm particles. (The reported experimental uncertainties are 1σ standard deviations over each measurement period.)

GF calculations for PM_{all} utilized a combined size distribution from the SEMS and the APS, with the merge point at a $d_{p,m}$ = 1000 nm. The APS sampled at a separate time from the CRD (see Table 1). The CRD set-up also required dilution due to the 3 LPM required for the cyclone and a total pull of ~6.3 LPM. Therefore, a dilution correction was applied to the APS distributions to account for the different sampling scheme. Although this adjustment adds some uncertainty to the PM_{all} size distributions, the concentrations at larger sizes were very small and thus had minimal influence on the derived *GF*s. For the $PM_{2.5}$ sampling periods, only SEMS distributions were used.

3 Results

3.1 Size Distributions and Dry Particle Optical Closure

The daily and study average merged size distributions for each MART are shown in Figure 2A (indoor MART) and Figure 2B (outdoor MART). The day-to-day variations in the size distributions were generally small. The average SSA particle number-weighted size distributions from both MARTs peaked around $d_{p,m}$ = 100 nm and were relatively broad. The observed concentration of supermicron particles ($d_{p,m}$ > 1000 nm) was somewhat lower than that previously reported from a MART (Stokes et al., 2013) and likely reflects greater gravitational losses of supermicron particles in the long sampling line used here (Figure S4). Since the hygroscopicity measurements discussed in this study are based on measurements made using polydisperse distributions, it is useful to determine the effective, scattering-weighted particle diameters that characterize the MART size distributions. The study average integrated scattering for each MART was calculated from Mie theory using the observed dry particle size distributions (Figure 2C). The

$d_{p,m}$ at which 50% of the total scattering occurs were 570 nm for the outdoor MART and 530 nm for the indoor MART and particles with $d_{p,m}$ > 1000 nm contributed <10% of the total scattering in both MARTs, indicating that the derived *GF*(85%) values for these two experiments are most sensitive to submicron particles with $d_{p,m}$ values between about 400 nm and 800 nm.

The extent of agreement between the observed b_{sca} for dry particles and the values calculated from Mie theory using measured size distributions (Equation 3) has been assessed (Figure S5). The calculated b_{sca} are ~15% lower than the observed b_{sca} for both PM_{all} and $PM_{2.5}$, which is outside the combined uncertainty for the CRD and size distribution measurements (which is ~11% from error propagation). Some of the difference may result from differential losses between or within the sizing instruments and the CRD, although this seems generally unlikely to explain the entire difference, as losses of particles in the submicron range should be small. There is greater scatter in the PM_{all} light scattering comparison than there is from the $PM_{2.5}$ comparison, which likely results both from the APS measurements being made at a different time than the CRD and SEMS measurements and the need for dilution correction. Some of the difference between the observed and calculated b_{sca} may be attributable to the assumption of spherical particles in the calculations, although similar closure was obtained (within 16%) between observed and calculated b_{sca} for atomized NaCl, suggesting that this is unlikely to explain the difference. It is possible that the diameters measured by the SEMS may have been too small. Wiedensohler et al. (2012) reported that sizing errors between instruments can be up to 10%. If the measured diameters are increased by 8%, then a 1:1 agreement between the measured and calculated extinction values is obtained. However, tests conducted during the study in which a 2nd DMA was used to size-select monodisperse particles in the range 100-300 nm indicated agreement between the instruments to within 1%. Additional tests after the study using 220 nm monodisperse polystyrene latex spheres (PSLs) demonstrated the SEMS sizing was good to better than 1%, suggesting that sizing inaccuracies cannot explain the difference absent some fundamental problem with the data inversion procedure for size distributions (Lopez-Yglesias et al., 2014), which seems unlikely. Uncertainty in the assumed RI value for the dry particles may explain a small fraction (<5%) of the difference. Additionally, if the dry particles had retained some water in the CRD but not the SEMS, then the observed b_{sca} would be larger than the calculated value. However, the RH in the CRD dry channel is much lower than the efflorescence RH for NaCl (~45% (Biskos et al., 2006)), and thus it seems unlikely that residual water would have contributed substantially to the

difference. Regardless of the explicit reason for the difference in calculated and observed absolute values of b_{sca}, since the calculation of f(RH) depends on the ratio between the b_{sca} for wet and dry particles, such absolute differences do not strongly affect the retrieval of *GF*(85%) values. We have tested the sensitivity of the retrieval method to an 8% increase in the particle diameters. The retrieved *GF* values are increased by a marginal amount (0.015-0.03) when the diameters are increased, and thus such potential sizing uncertainty does not affect the main conclusions presented here.

3.1 Indoor MART

The temporal variation in Chl-a concentrations, the derived *GF*(85%) and various particle composition metrics are shown in Figure 3 for the indoor MART. As has been previously observed in microcosm experiments, the measured Chl-a time series exhibits a distinct peak (Lee et al., 2015), which in this case occurred on 16 July at a value of 10 μg L^{-1}. This Chl-a concentration is around the upper end of values observed for large phytoplankton blooms observed in the oceans, in particular near coastal regions (O'Reilly et al., 1998). After the peak the Chl-a concentration dropped relatively quickly to around 1.5 μg L^{-1} (15% of the peak) and then eventually to ~1.4 μg L^{-1} (14% of the peak). The DOC concentrations varied from 240 to 350 μM C, increasing rapidly when the Chl-a concentration peaked and then staying relatively constant around 320 μM (Figure S6A). The peak DOC range is somewhat larger than values typically observed for blooms in the ocean, which are only ~130 - 250 μM C (Kirchman et al., 1991; Norrman et al., 1995). The temporal variation in heterotrophic bacteria concentration was similar to that for DOC, and heterotrophic bacteria concentrations ranged from ~1 x 10^6 to 1.2 x 10^7 mL^{-1} (Figure S6A), which is comparable to concentrations observed in the ocean (Li, 1998).

The *GF*(85%) values determined for the indoor MART ranged from 1.79 to 1.9 and exhibited distinct temporal variations, decreasing from 1.88 ± 0.04 on 16 July, just as the Chl-a peaked, to a minimum range of 1.79 ± 0.03 to 1.80 ± 0.01 from 17 July to 18 July when the Chl-a concentration dropped to 3.41 ± 1.89 μg L^{-1}, and then recovering back to 1.90 ± 0.03 on 7/20 (Figure 3A). The range of these values is 10-15% lower than the value of ~2.1 for pure (inorganic) sea salt (Ming and Russell, 2001). There is a one day lag between the peak in Chl-a and the (temporary) depression in *GF*(85%).

The NR-OM volume fractions of SSA varied from 0.29 to 0.50 throughout the course of the indoor MART microcosm experiment (Figure 3). The observation of such large ε_{org} values is consistent with the substantial depressions in the *GF*(85%) values relative to pure, inorganic sea salt (2.1). The temporal variation in the ε_{org} was generally similar to that of the *GF*(85%) values, with smaller *GF*(85%) values corresponding to larger ε_{org} values, although the peak in ε_{org} is somewhat sharper than the dip in the *GF*(85%). The inverse relationship between the *GF*(85%) and ε_{org} is consistent with organic compounds being less hygroscopic than sea salt. The O:C ratio of the NR-OM had an average value of 0.25 ± 0.05 (1σ), which is similar to the value of 0.20 ± 0.08 reported by Frossard et al. (2014) for primary NR-OM that was generated from the open ocean using the "sea sweep" (Bates et al., 2012). The O:C ratio of NR-OM in the indoor MART generally increased with time, from 0.17 to 0.30, but also exhibited a temporary decrease on 17 July, the day when the *GF*(85%) and ε_{org} both first dropped. Since O:C often correlates with hygroscopicity for organics (at least for multi-component mixtures), this behavior may indicate a general increase in the hygroscopicity of the NR-OM with time (Cappa et al., 2011; Massoli et al., 2010). However, since the hygroscopicity of organic aerosol with O:C values in this range has generally been found to be small, the observed variations in O:C may not have a noticeable impact on the overall behavior of the *GF*(85%) values.

The explicit co-variation of ε_{org} and the *GF*(85%) values is shown in Figure 4. Assuming that volume mixing rules apply (i.e. the Zdanovskii-Stokes-Robinson (ZSR) mixing rules (Stokes and Robinson, 1966)), the overall, effective *GF* (GF_{obs}) can be estimated as:

$$GF_{obs} = \left((1 - \varepsilon_{org}) \cdot {GF_{sea\ salt}}^3 + \varepsilon_{org} \cdot {GF_{org}}^3\right)^{1/3} \quad (5)$$

where GF_{org} is the *GF* value for pure OM and $GF_{sea\ salt}$ is the *GF* value expected for pure sea salt. The ZSR line connecting $GF_{sea\ salt}$(85%) = 2.1 and GF_{org}(85%) = 1.0 provides the minimum value expected for any fraction of OM relative to sea salt. Low GF_{org}(85%) values (~1.0) have been observed for fatty acids (Vesna et al., 2008), which have been found in SSA particles in the atmosphere (Mochida et al., 2002) and were observed in SSA produced in a related mesocosm experiment (Wang et al., 2015; Cochran et al., 2016). Values above this line indicate that the *GF* of the OM in the sampled SSA particles is, on average, greater than 1. Equation 5 was fit to the

data shown in Figure 4 to determine an average value for $GF_{org}(85\%)$ for the indoor MART. The best-fit $GF_{org}(85\%)$ was 1.16 ± 0.09, which falls between GF_{org} = 1.0 expected for non-hygroscopic OM, such as fatty acids, and GF_{org} expected for more soluble OM, such as sugars (e.g. $GF_{org}(85\%)$ = 1.24 ± 0.04 has been observed for glucose (Mochida and Kawamura, 2004)). (The uncertainty on $GF_{org}(85\%)$ is the fit uncertainty and does not account for uncertainties in either the *CE* for SSA particles or in ρ_{OM}.) This value for GF_{org} can be interpreted as an optically-weighted average for the OM component of the SSA particles sampled here. Although the derived GF_{org} values are reasonable, as the *CE* is relatively uncertain for sea spray particles (Ovadnevaite et al., 2012; Frossard et al., 2014) and the ρ_{OM} is also uncertain, the derived value for GF_{org} should be viewed as suggestive only.

One important issue to consider in assessing the quantitative nature of the derived $GF_{org}(85\%)$ value is that the mass-weighted organic fractions used to determine ε_{org} do not necessarily have the same weighting with respect to particle size as do the *GF*(85%) values. The scattering-weighted median diameter, relevant to the *GF*(85%) measurements, was $d_{p,m}$ = 530 nm. The mass-weighted size distribution of OM can be estimated from the size distribution of a particular tracer ion in the AMS mass spectrum, specifically the ion at m/z = 43, which is indicative of total organic mass (Figure S7). (Interference from the large signal contribution from inorganic ions prohibited explicit determination of the total NR-OM size distribution, and thus only the m/z = 43 ion is used.) The peak in the NR-OM mode occurs at d_{va} ~ 1 μm, which corresponds to $d_{p,m}$ = 560 nm. This is comparable to the scattering-weighted median diameter, suggesting that the temporal variations in the *GF*(85%) and ε_{org} can be compared. However, the AMS aerodynamic lens imposes a 50% cut diameter of ~1 μm (Canagaratna et al., 2007) and thus the observed peak in m/z 43 likely occurs at a diameter that is somewhat too small compared to the actual distribution.

There was also a strong temporal correlation observed between the *GF*(85%) values and the number fractions of ATOFMS mass spectra categories. Specifically, the decrease in *GF*(85%) values after the bloom peak corresponded to a shift from particles that generated mass spectra dominated by sea salt ion markers (SS type) to particles with strong spectral signatures indicative of organic or biological influence (SSOC and Mg type). (The measurements made just after nutrient addition on 9 July are a notable exception, discussed below). The inverse relationship between the *GF*(85%) and the SS type particle spectra is consistent with the inverse relationship

between the *GF*(85%) and ε_{org}, providing additional confidence that the temporal variations in *GF*(85%) are driven by variations in particle composition. The SSOC mass spectral type is identified in large part by the presence of carbon-containing peaks (CN^- and CNO^-) and K^+ and Ca^+ in the mass spectrum (see Figure S2). The Mg-type spectra are characterized by their large Mg^+ peak, which has been previously attributed to the presence of biological material (e.g. bacteria) (Guasco et al., 2013; Prather et al., 2013), as well as by smaller Ca^+ and K^+ peaks (Figure S2). Both the SSOC and Mg spectral types are depleted in peaks corresponding to Na or NaCl. It is important to note, however, that dried SSA particles sampled by the ATOFMS can be spatially chemically heterogeneous, with shells depleted in Na and rich in Mg, K, and Ca (Ault et al., 2013). Thus, some fraction of the particles identified as having Mg or SSOC type spectra may be partially explained by the incomplete ionization of sea salt particles (Sultana et al., In Prep.). However, variations in the thickness of this Na-depleted shell likely reflect variations in the total particle organic content. Therefore, increases in the fraction of SSOC or Mg type mass spectra generated suggest a net increase in SSA particle organic content. On 9 July a substantial fraction of particles containing large Fe^+ peaks were observed; on all other days the Fe spectral-type particle fraction was negligible. The Fe spectral-type particles may have had an influence on the observed *GF*(85%) values when present with high relative abundance. However, their large fraction on 9 July is a result of nutrient addition and not biological changes in the seawater.

3.2 Outdoor MART

The temporal variation in Chl-a concentrations, the derived *GF*(85%) values and various particle composition metrics are shown in Figure 5 for the outdoor MART. Like the indoor MART, the Chl-a concentrations exhibited a characteristic rise and fall for the microcosm experiment. However, the maximum Chl-a concentration was 51 μg L^{-1}, which 5 times higher than the indoor MART and likely due to greater PAR in the outdoor MART. Such high Chl-a concentrations are well above those typically observed in the ocean. However, the Chl-a concentration rapidly declined to 6 μg L^{-1} two days after the peak and then continued to decrease over the next week to <1.5 μg L^{-1}. Both DOC and heterotrophic bacteria concentrations increased as the bloom progressed until they stabilized around the point when Chl-a concentrations had returned approximately to their pre-bloom levels, with DOC concentrations ranging from 200 to 300 μM C and heterotrophic bacteria concentrations from 1 x 10^6 to a peak of 1.7 x 10^7 mL^{-1} (Figure S6B).

The *GF*(85%) values ranged from a maximum of 1.99 ± 0.03 to a minimum of 1.78 ± 0.04, again lower than what would be expected for pure sea salt (by 5-15%). Unfortunately, no pre-bloom measurements were possible for this experiment, with the first particle measurements made for all instruments when the Chl-a concentration was peaking. The smallest *GF*(85%) values were observed towards the end of the microcosm, when the Chl-a concentrations were at their lowest point (< 1.5 μg L^{-1}). The *GF*(85%) values exhibited two sequential decreases after the Chl-a peak, the first after 3 days and the second after 6 days. The range of *GF*(85%) values for the SSA particles from the outdoor MART were similar to those for the indoor MART

The observed ε_{org} values for the SSA particles were similarly comparable to the indoor MART (0.26 to 0.46). In general, decreases in *GF*(85%) values corresponded to increases in ε_{org} values, with the exception of the measurements on 7/30 (Figure 5C). Following the peak in Chl-a, the ε_{org} values increase gradually over a few days, then stabilize, and finally exhibit an additional increase six days after the bloom peak (Figure 5A). The temporal variations in ε_{org} tracks neither the Chl-a nor DOC concentrations. This suggests that, perhaps, biological processing and its impact on the composition of organics in the sea water, more so than absolute organic concentrations, is important for determining the abundance of organic matter transferred into SSA particles (Rinaldi et al., 2013; Lee et al., 2015; Quinn et al., 2014). However, further experiments will be needed to confirm this hypothesis.

Values of GF_{org}(85%) have again been estimated using the ZSR relationship (Eqn. 5) and the observed *GF*(85%) and ε_{org}. Assuming $GF_{sea\ salt}$ (85%) = 2.1, the derived GF_{org}(85%) = 1.23 ± 0.10 (Figure 4). This GF_{org}(85%) for the outdoor MART is comparable to that obtained from the indoor MART, suggesting that the OM generated from the outdoor MART has similar hygroscopicity as the OM sampled from the indoor MART.

As with the indoor MART, there was a reasonable temporal correlation between the *GF*(85%) values and the number concentration of SS spectral-type particles from the ATOFMS. The two most abundant non-SS particle mass spectra types were SSOC-type and Mg-type, with all other types contributing negligibly. This is again an indication that the temporal variation in the *GF*(85%) values corresponds to an evolution of the composition of the SSA particle population, and is consistent with the variation in ε_{org}.

4 Implications and Conclusions

The two MART microcosm studies provide two case studies relating variations in the optically-weighted *GF*(85%) values and SSA particle composition for predominately submicrometer SSA particles. For both microcosms, clear depression of the *GF*(85%) values, relative to that for pure sea salt, occurred following the peak in Chl-a concentrations and upon the death of both phytoplankton blooms, but with differing time lags between peak Chl-a and the minimum *GF*(85%) between the experiments. This depression in *GF*(85%) values is consistent with large ε_{org} (0.25 – 0.50) values estimated using the NR-OM/PM_1. The similar temporal variations in *GF*(85%) and ε_{org}, as well as with the ATOFMS particle mass spectra types, demonstrates a clear link between SSA hygroscopicity and composition. For a given microcosm experiment, the estimated hygroscopicity of OM components are similar, with *GF*(85%) = 1.16 for the indoor MART and 1.23 for the outdoor MART.

The observations here demonstrate that the climate impacts of marine-derived organic compounds can go beyond their demonstrated ability to influence cloud condensation nuclei efficacy (Quinn et al., 2014; Collins et al., 2013), additionally affecting the efficiency with which SSA particles scatter solar radiation. This was previously suggested by the ambient measurements of Vaishya et al. (2013), who observed substantial differences in *GF*(90%) and *f*(RH) values for submicron particles having very different ε_{org} fractions in what were identified as clean marine air masses. (Their *GF*(90%) values were measured using a hygroscopic tandem DMA (HT-DMA) for size-selected particles with 35 nm $\leq d_{p,m} \leq$ 165 nm. Their *f*(RH) values were measured for PM_1.) They observed that increases in ε_{org} had no effect on the *GF*(90%) until a threshold ε_{org} was reached, specifically ε_{org} > ~55%. Below this value, they measured *GF*(90%) value of ~ 2.3, which is the expected value for pure sea salt at *RH* = 90%. Above this value, the observed a rapid fall off in *GF*(90%) to a plateau at 1.22. This reported behavior differs from that observed for nascent SSA particles sampled in the current study. Here, substantial depressions in *GF*(85%) (and *f*(RH)) relative to inorganic sea salt were observed when the ε_{org} was only ~25%, and a co-variation between *GF*(85%) and ε_{org} (and the ATOFMS SS spectral-type fraction) was observed. One plausible reason for this difference is that nascent (freshly-emitted) SSA particles are measured here whereas *Vaishya* et al. (2013) measured ambient particles that could be subject to photochemical processing. Secondary organic aerosol formed from gases, such as monoterpenes and isoprene, emitted from the ocean (Shaw et al., 2010) could have contributed to the NR-OM,

although Vaishya et al. (2013) argue that this influence was negligible based on the literature. Emission rates of such species from the ocean and their relationship with oceanic processes are not well established. Although *Vaishya* et al. (2013) attempted to remove the influence of secondary organics in their analysis (as well as the influence of non-sea salt sulfate), it is possible that their analysis was complicated by the impacts of atmospheric processing. Another key difference is that relationship between the *GF*(85%) values and ε_{org} observed in the current study is consistent with ZSR behavior, while Vaishya et al. reported "bistable" behavior of the *GF*(90%) values as a function ε_{org} (i.e. the flat behavior at ε_{org} < 55% and the steep fall off above). The physical basis of this bistable behavior, and the functional form implied by their measurements, is not easily explained. Finally, the *GF*(90%) measurements by Vaishya et al. were made for particles with $d_{p,m}$ < 165 nm, while the composition was characterized with an HR-AMS. It is possible that size mismatch between these measurements influenced their analysis. Mass-weighted size distributions were not shown by Vaishya et al. (2013), however Frossard et al. show mass-weighted size distributions for ambient particles sampled in the remote marine boundary layer that suggest that much of the organic mass is contained in particles > 165 nm. Our results clearly indicate that compositional changes to nascent SSA particles, driven by variation in physical and biochemical processes in seawater, can impact the influence of water uptake on scattering by submicron SSA even when ε_{org} < 55%. The comparison with the *Vaishya et al.* (2013) measurements suggests that this initial state can be further modified through atmospheric processing.

The implications of these results are explored here through calculations of the net decrease (relative to pure sea salt) in the average per particle scattering that would theoretically result from increasing amounts of OM in SSA particles, assuming that the SSA particles follow the ZSR mixing rules (see Figure 6). This has been done for different assumed $GF(85\%)_{org}$ values as a function of ε_{org} using the average size distribution for the outdoor MART shown in Figure 2B. Given the particle size distributions measured here, this assessment pertains to submicron SSA, not the entire SSA particle size distribution observed over the ocean (which includes contributions from supermicron particles (Kleefeld et al., 2002)). The range of ε_{org} and $GF_{org}(85\%)$ values determined here (about 0.25-0.50 and 1.16-1.23, respectively) correspond to decreases in scattering of about 15 to 30%. Thus, climate models that assume SSA particles behave like pure sea salt or NaCl (Stier et al., 2005; Schmidt et al., 2006) may over-predict SSA particle scattering,

dependent upon the exact RH fields in the model. However, the range of ε_{org} observed here, ~0.25 to 0.50, may be larger than is typical in the ambient marine atmosphere, given that the MART bloom experiments are more representative of regions of the ocean with high biological activity. For example, O'Dowd et al. (2004) observed mass fractions of ~0.40 organic matter for SSA particles with aerodynamic diameters between 0.5 and 1 μm during periods with high biological productivity, but < 5% for periods with low productivity. Regardless, the results presented here suggest that OM in SSA particles may have a non-negligible, yet variable impact on the light scattering by SSA particles in the ambient atmosphere (Figure S8). Most likely, the simulated cooling effect of SSA particles due to aerosol-radiation interactions (i.e. the "direct effect") would be decreased relative to the assumption that all SSA behaves as sea salt. Recent climate modeling studies (Partanen et al., 2014; O'Dowd et al., 2008) have attempted to account for variability in OM fractions of SSA particles by parameterizing OM fraction as a function of Chl-a. However, relating the OM fraction of SSA particles to simple ocean biological metrics like Chl-a still remains challenging, as these metrics are often insufficient predictors for SSA particle composition (Quinn et al., 2014; Wang et al., 2015), and the measurements reported here indicate a clear lag between the peak in Chl-a and the minimum in the *GF*(85%) values. Quantitative understanding of the climate impacts of SSA particles will require further understanding of the timing and relationships between ocean biogeochemistry and SSA properties.

5 Acknowledgments

This study was funded by the Center for Aerosol Impacts on Climate and Environment (CAICE), a NSF Center for Chemical Innovation (CHE-1305427). The authors thank all IMPACTS participants and the SIO hydraulics facility staff. SDF and CDC additionally thank the students in ECI 247L during spring quarter 2015 at UC Davis, who validated the SEMS sizing.

References

Ault, A. P., Guasco, T. L., Ryder, O. S., Baltrusaitis, J., Cuadra-Rodriguez, L. A., Collins, D. B., Ruppel, M. J., Bertram, T. H., Prather, K. A., and Grassian, V. H.: Inside versus outside: Ion redistribution in nitric acid reacted sea spray aerosol particles as determined by single particle analysis, Journal of the American Chemical Society, 135, 14528-14531, 10.1021/ja407117x, 2013.

Bates, T., Quinn, P., Frossard, A., Russell, L., Hakala, J., Petäjä, T., Kulmala, M., Covert, D., Cappa, C., and Li, S. M.: Measurements of ocean derived aerosol off the coast of california, Journal of Geophysical Research: Atmospheres (1984–2012), 117, 2012.

Biskos, G., Malinowski, A., Russell, L., Buseck, P., and Martin, S.: Nanosize effect on the deliquescence and the efflorescence of sodium chloride particles, Aerosol Science and Technology, 40, 97-106, 10.1080/02786820500484396, 2006.

Bouvet, M., Hoepffner, N., and Dowell, M. D.: Parameterization of a spectral solar irradiance model for the global ocean using multiple satellite sensors, Journal of Geophysical Research: Oceans (1978–2012), 107, 8-1-8-18, 10.1029/2001JC001126, 2002.

Canagaratna, M. R., Jayne, J. T., Jimenez, J. L., Allan, J. D., Alfarra, M. R., Zhang, Q., Onasch, T. B., Drewnick, F., Coe, H., Middlebrook, A., Delia, A., Williams, L. R., Trimborn, A. M., Northway, M. J., DeCarlo, P. F., Kolb, C. E., Davidovits, P., and Worsnop, D. R.: Chemical and microphysical characterization of ambient aerosols with the aerodyne aerosol mass spectrometer, Mass Spectrometry Reviews, 26, 185-222, 10.1002/mas.20115, 2007.

Cappa, C. D., Che, D. L., Kessler, S. H., Kroll, J. H., and Wilson, K. R.: Variations in organic aerosol optical and hygroscopic properties upon heterogeneous oh oxidation, Journal of Geophysical Research: Atmospheres, 116, D15204, 10.1029/2011JD015918, 2011.

Cappa, C. D., Onasch, T. B., Massoli, P., Worsnop, D., Bates, T. S., Cross, E., Davidovits, P., Hakala, J., Hayden, K., Jobson, B. T., Kolesar, K. R., Lack, D. A., Lerner, B., Li, S. M., Mellon, D., Nuaanman, I., Olfert, J., Petaja, T., Quinn, P. K., Song, C., Subramanian, R., Williams, E. J., and Zaveri, R. A.: Radiative absorption enhancements due to the mixing state of atmospheric black carbon Science, 337, 1078-1081, 10.1126/science.1223447, 2012.

Carslaw, K., Lee, L., Reddington, C., Pringle, K., Rap, A., Forster, P., Mann, G., Spracklen, D., Woodhouse, M., and Regayre, L.: Large contribution of natural aerosols to uncertainty in indirect forcing, Nature, 503, 67-71, 10.1038/nature12674, 2013.

Cochran, R., Laskina, O., Jayarathne, T., Laskin, A., Laskin, J., Lin, P., Sultana, C. M., Moore, K. A., Cappa, C., Bertram, T., Prather, K. A., and Grassian, V. H.: Analysis of organic anionic surfactants in fine (pm2.5) and coarse (pm10) fractions of freshly emitted sea spray aerosol, Environmental Science & Technology, 50 2477-2486, 10.1021/acs.est.5b04053, 2016.

Collins, D. B., Ault, A. P., Moffet, R. C., Ruppel, M. J., Cuadra-Rodriguez, L. A., Guasco, T. L., Corrigan, C. E., Pedler, B. E., Azam, F., and Aluwihare, L. I.: Impact of marine biogeochemistry on the chemical mixing state and cloud forming ability of nascent sea spray aerosol, Journal of Geophysical Research: Atmospheres, 118, 8553-8565, 10.1002/jgrd.50598, 2013.

Cruz, C. N., and Pandis, S. N.: Deliquescence and hygroscopic growth of mixed inorganic-organic atmospheric aerosol, Environmental Science & Technology, 34, 4313-4319, 10.1021/es9907109, 2000.

Dusek, U., Frank, G., Hildebrandt, L., Curtius, J., Schneider, J., Walter, S., Chand, D., Drewnick, F., Hings, S., and Jung, D.: Size matters more than chemistry for cloud-nucleating ability of aerosol particles, Science, 312, 1375-1378, 10.1126/science.1125261, 2006.

Facchini, M. C., Rinaldi, M., Decesari, S., Carbone, C., Finessi, E., Mircea, M., Fuzzi, S., Ceburnis, D., Flanagan, R., and Nilsson, E. D.: Primary submicron marine aerosol dominated by insoluble organic colloids and aggregates, Geophysical Research Letters, 35, 17814, 10.1029/2008GL034210, 2008.

Farmer, D. K., Cappa, C. D., and Kreidenweis, S. M.: Atmospheric processes and their controlling influence on cloud condensation nuclei activity, Chemical Reviews, 115, 4199–4217, 10.1021/cr5006292, 2015.

Frossard, A. A., Russell, L. M., Massoli, P., Bates, T. S., and Quinn, P. K.: Side-by-side comparison of four techniques explains the apparent differences in the organic composition of generated and ambient marine aerosol particles, Aerosol Science and Technology, 48, v-x, 10.1080/02786826.2013.879979, 2014.

Fuentes, E., Coe, H., Green, D., and McFiggans, G.: On the impacts of phytoplankton-derived organic matter on the properties of the primary marine aerosol–part 2: Composition, hygroscopicity and cloud condensation activity, Atmospheric Chemistry and Physics, 11, 2585-2602, 10.5194/acp-11-2585-2011, 2011.

Gard, E. E., Kleeman, M. J., Gross, D. S., Hughes, L. S., Allen, J. O., Morrical, B. D., Fergenson, D. P., Dienes, T., Galli, M. E., Johnson, R. J., Cass, G. R., and Prather, K. A.: Direct observation of heterogeneous chemistry in the atmosphere, Science, 279, 1184-1187, 10.1126/science.279.5354.1184, 1998.

Guasco, T. L., Cuadra-Rodriguez, L. A., Pedler, B. E., Ault, A. P., Collins, D. B., Zhao, D., Kim, M. J., Ruppel, M. J., Wilson, S. C., and Pomeroy, R. S.: Transition metal associations with primary biological particles in sea spray aerosol generated in a wave channel, Environmental Science & Technology, 48, 1324-1333, 10.1021/es403203d, 2013.

Hansson, H.-C., Rood, M., Koloutsou-Vakakis, S., Hämeri, K., Orsini, D., and Wiedensohler, A.: Nacl aerosol particle hygroscopicity dependence on mixing with organic compounds, Journal of Atmospheric Chemistry, 31, 321-346, 10.1023/A:1006174514022, 1998.

Haywood, J., Ramaswamy, V., and Soden, B.: Tropospheric aerosol climate forcing in clear-sky satellite observations over the oceans, Science, 283, 1299-1303, 10.1126/science.283.5406.1299, 1999.

Hegg, D., Covert, D., and Jonsson, H.: Measurements of size-resolved hygroscopicity in the california coastal zone, Atmospheric Chemistry and Physics, 8, 7193-7203, 10.5194/acp-8-7193-2008, 2008.

IPCC: Climate change 2013: The physical science basis. Contribution of working group i to the fifth assessment report of the intergovernmental panel on climate change, Cambridge University Press, Cambridge, United Kingdom and New York, NY, USA, 1535 pp., 2013.

Keene, W. C., Maring, H., Maben, J. R., Kieber, D. J., Pszenny, A. A., Dahl, E. E., Izaguirre, M. A., Davis, A. J., Long, M. S., and Zhou, X.: Chemical and physical characteristics of nascent aerosols produced by bursting bubbles at a model air-sea interface, Journal of Geophysical Research: Atmospheres (1984–2012), 112, D21202, 10.1029/2007JD008464, 2007.

Kirchman, D. L., Suzuki, Y., Garside, C., and Ducklow, H. W.: High turnover rates of dissolved organic carbon during a spring phytoplankton bloom, Nature, 352, 612-614, 10.1038/352612a0, 1991.

Kleefeld, C., O'Dowd, C. D., O'Reilly, S., Jennings, S. G., Aalto, P., Becker, E., Kunz, G., and de Leeuw, G.: Relative contribution of submicron and supermicron particles to aerosol light scattering in the marine boundary layer, Journal of Geophysical Research: Atmospheres, 107, PAR 8-1-PAR 8-13, 10.1029/2000JD000262, 2002.

Kulkarni, P., Baron, P. A., and Willeke, K.: Aerosol measurement: Principles, techniques, and applications, John Wiley & Sons, 2011.

Langridge, J. M., Richardson, M. S., Lack, D., Law, D., and Murphy, D. M.: Aircraft instrument for comprehensive characterization of aerosol optical properties, part i: Wavelength-dependent optical extinction and its relative humidity dependence measured using cavity ringdown spectroscopy, Aerosol Science and Technology, 45, 1305-1318, 10.1080/02786826.2011.592745, 2011.

Laskina, O., Morris, H. S., Grandquist, J. R., Qin, Z., Stone, E. A., Tivanski, A. V., and Grassian, V. H.: Size matters in the water uptake and hygroscopic growth of atmospherically relevant multicomponent aerosol particles, The Journal of Physical Chemistry A, 119, 4489–4497, 10.1021/jp510268p, 2015.

Lawler, M., Whitehead, J., O'Dowd, C., Monahan, C., McFiggans, G., and Smith, J.: Composition of 15–85 nm particles in marine air, Atmospheric Chemistry and Physics, 14, 11557-11569, 10.5194/acp-14-11557-2014, 2014.

Lee, C., Sultana, C. M., Collins, D. B., Santander, M. V., Axson, J. L., Malfatti, F., Cornwell, G. C., Grandquist, J. R., Deane, G. B., Stokes, M. D., Azam, F., Grassian, V. H., and Prather, K. A.: Advancing model systems for fundamental laboratory studies of sea spray aerosol using the microbial loop, The Journal of Physical Chemistry A, 119 8860–8870, 10.1021/acs.jpca.5b03488, 2015.

Lewis, E. R., and Schwartz, S. E.: Sea salt aerosol production: Mechanisms, methods, measurements, and models-a critical review, American Geophysical Union, 2004.

Li, W. K.: Annual average abundance of heterotrophic bacteria and synechococcus in surface ocean waters, Limnology and Oceanography, 43, 1746-1753, 10.4319/lo.1998.43.7.1746, 1998.

Lopez-Yglesias, X. F., Yeung, M. C., Dey, S. E., Brechtel, F. J., and Chan, C. K.: Performance evaluation of the brechtel mfg. Humidified tandem differential mobility analyzer (bmi htdma) for studying hygroscopic properties of aerosol particles, Aerosol Science and Technology, 48, 969-980, 10.1080/02786826.2014.952366, 2014.

Massoli, P., Lambe, A., Ahern, A., Williams, L., Ehn, M., Mikkilä, J., Canagaratna, M., Brune, W., Onasch, T., and Jayne, J.: Relationship between aerosol oxidation level and hygroscopic properties of laboratory generated secondary organic aerosol (soa) particles, Geophysical Research Letters, 37, L24801, 10.1029/2010GL045258, 2010.

Ming, Y., and Russell, L. M.: Predicted hygroscopic growth of sea salt aerosol, Journal of Geophysical Research: Atmospheres, 106, 28259-28274, 10.1029/2001JD000454, 2001.

Mochida, M., Kitamori, Y., Kawamura, K., Nojiri, Y., and Suzuki, K.: Fatty acids in the marine atmosphere: Factors governing their concentrations and evaluation of organic films on sea-salt particles, Journal of Geophysical Research: Atmospheres (1984–2012), 107, AAC 1-1–AAC 1-10, 2002.

Mochida, M., and Kawamura, K.: Hygroscopic properties of levoglucosan and related organic compounds characteristic to biomass burning aerosol particles, Journal of Geophysical Research: Atmospheres, 109, n/a-n/a, 10.1029/2004jd004962, 2004.

Modini, R. L., Harris, B., and Ristovski, Z.: The organic fraction of bubble-generated, accumulation mode sea spray aerosol (ssa), Atmospheric Chemistry and Physics, 10, 2867-2877, 10.5194/acp-10-2867-2010, 2010.

Norrman, B., Zwelfel, U. L., Hopkinson, C. S., and Brian, F.: Production and utilization of dissolved organic carbon during an experimental diatom bloom, Limnology and Oceanography, 40, 898-907, 10.4319/lo.1995.40.5.0898, 1995.

O'Dowd, C. D., Facchini, M. C., Cavalli, F., Ceburnis, D., Mircea, M., Decesari, S., Fuzzi, S., Yoon, Y. J., and Putaud, J.-P.: Biogenically driven organic contribution to marine aerosol, Nature, 431, 676-680, 10.1038/nature02959, 2004.

O'Dowd, C. D., Langmann, B., Varghese, S., Scannell, C., Ceburnis, D., and Facchini, M. C.: A combined organic-inorganic sea-spray source function, Geophysical Research Letters, 35, L01801, 10.1029/2007GL030331, 2008.

O'Reilly, J. E., Maritorena, S., Mitchell, B. G., Siegel, D. A., Carder, K. L., Garver, S. A., Kahru, M., and McClain, C.: Ocean color chlorophyll algorithms for seawifs, Journal of Geophysical Research: Oceans, 103, 24937-24953, 10.1029/98JC02160, 1998.

Ovadnevaite, J., Ceburnis, D., Martucci, G., Bialek, J., Monahan, C., Rinaldi, M., Facchini, M. C., Berresheim, H., Worsnop, D. R., and O'Dowd, C.: Primary marine organic aerosol: A dichotomy of low hygroscopicity and high ccn activity, Geophysical Research Letters, 38, L21806, 10.1029/2011GL048869, 2011.

Ovadnevaite, J., Ceburnis, D., Canagaratna, M., Berresheim, H., Bialek, J., Martucci, G., Worsnop, D. R., and O'Dowd, C.: On the effect of wind speed on submicron sea salt mass concentrations and source fluxes, Journal of Geophysical Research-Atmospheres, 117, 10.1029/2011jd017379, 2012.

Park, J. Y., Lim, S., and Park, K.: Mixing state of submicrometer sea spray particles enriched by insoluble species in bubble-bursting experiments, Journal of Atmospheric and Oceanic Technology, 31, 93-104, 10.1175/JTECH-D-13-00086.1, 2014.

Partanen, A.-I., Dunne, E., Bergman, T., Laakso, A., Kokkola, H., Ovadnevaite, J., Sogacheva, L., Baisnée, D., Sciare, J., and Manders, A.: Global modelling of direct and indirect effects of sea spray aerosol using a source function encapsulating wave state, Atmospheric Chemistry and Physics, 14, 11731-11752, 10.5194/acp-14-11731-2014, 2014.

Petters, M., and Kreidenweis, S.: A single parameter representation of hygroscopic growth and cloud condensation nucleus activity, Atmospheric Chemistry and Physics, 7, 1961-1971, 10.5194/acp-7-1961-2007, 2007.

Pilinis, C., Pandis, S. N., and Seinfeld, J. H.: Sensitivity of direct climate forcing by atmospheric aerosols to aerosol size and composition, Journal of Geophysical Research: Atmospheres, 100, 18739-18754, 10.1029/95JD02119, 1995.

Pomeroy, L. R., Williams, P. J. l. B., Azam, F., and Hobbie, J. E.: The microbial loop, Oceanography, 20, 28-33, 10.5670/oceanog.2007.45, 2007.

Prather, K. A., Bertram, T. H., Grassian, V. H., Deane, G. B., Stokes, M. D., DeMott, P. J., Aluwihare, L. I., Palenik, B. P., Azam, F., and Seinfeld, J. H.: Bringing the ocean into the

laboratory to probe the chemical complexity of sea spray aerosol, Proceedings of the National Academy of Sciences, 110, 7550-7555, 10.1073/pnas.1300262110, 2013.

Pratt, K. A., DeMott, P. J., French, J. R., Wang, Z., Westphal, D. L., Heymsfield, A. J., Twohy, C. H., Prenni, A. J., and Prather, K. A.: In situ detection of biological particles in cloud ice-crystals, Nature Geoscience, 2, 397-400, 10.1038/ngeo521, 2009.

Quinn, P. K., Bates, T. S., Schulz, K. S., Coffman, D. J., Frossard, A. A., Russell, L. M., Keene, W. C., and Kieber, D. J.: Contribution of sea surface carbon pool to organic matter enrichment in sea spray aerosol, Nature Geosci, 7, 228-232, 10.1038/ngeo2092, 2014.

Quinn, P. K., Collins, D. B., Grassian, V. H., Prather, K. A., and Bates, T. S.: Chemistry and related properties of freshly emitted sea spray aerosol, Chemical reviews, 10.1021/cr500713g, 2015.

Rinaldi, M., Fuzzi, S., Decesari, S., Marullo, S., Santoleri, R., Provenzale, A., Hardenberg, J., Ceburnis, D., Vaishya, A., and O'Dowd, C. D.: Is chlorophyll-a the best surrogate for organic matter enrichment in submicron primary marine aerosol?, Journal of Geophysical Research: Atmospheres, 118, 4964-4973, 10.1002/jgrd.50417, 2013.

Saxena, P., Hildemann, L. M., McMurry, P. H., and Seinfeld, J. H.: Organics alter hygroscopic behavior of atmospheric particles, Journal of Geophysical Research: Atmospheres (1984–2012), 100, 18755-18770, 10.1029/95JD01835, 1995.

Schmidt, G. A., Ruedy, R., Hansen, J. E., Aleinov, I., Bell, N., Bauer, M., Bauer, S., Cairns, B., Canuto, V., and Cheng, Y.: Present-day atmospheric simulations using giss modele: Comparison to in situ, satellite, and reanalysis data, Journal of Climate, 19, 153-192, 2006.

Sellegri, K., Villani, P., Picard, D., Dupuy, R., O'Dowd, C., and Laj, P.: Role of the volatile fraction of submicron marine aerosol on its hygroscopic properties, Atmospheric Research, 90, 272-277, 10.1016/j.atmosres.2008.04.004, 2008.

Shaw, S. L., Gantt, B., and Meskhidze, N.: Production and emissions of marine isoprene and monoterpenes: A review, Adv. Meteorol., 2010, 10.1155/2010/408696, 2010.

Skop, R. A., Viechnicki, J. T., and Brown, J. W.: A model for microbubble scavenging of surface-active lipid molecules from seawater, Journal of Geophysical Research: Oceans (1978–2012), 99, 16395-16402, 10.1029/94JC01199, 1994.

Stefan, R. L., and Szeri, A. J.: Surfactant scavenging and surface deposition by rising bubbles, Journal of colloid and interface science, 212, 1-13, 10.1006/jcis.1998.6037, 1999.

Stier, P., Feichter, J., Kinne, S., Kloster, S., Vignati, E., Wilson, J., Ganzeveld, L., Tegen, I., Werner, M., and Balkanski, Y.: The aerosol-climate model echam5-ham, Atmospheric Chemistry and Physics, 5, 1125-1156, 2005.

Stokes, M. D., Deane, G. B., Prather, K., Bertram, T. H., Ruppel, M. J., Ryder, O. S., Brady, J. M., and Zhao, D.: A marine aerosol reference tank system as a breaking wave analogue for the production of foam and sea-spray aerosols, Atmos. Meas. Tech., 6, 1085-1094, 10.5194/amt-6-1085-2013, 2013.

Stokes, R., and Robinson, R.: Interactions in aqueous nonelectrolyte solutions. I. Solute-solvent equilibria, The Journal of Physical Chemistry, 70, 2126-2131, 10.1021/j100879a010, 1966.

Sultana, C. M., Collins, D. B., Lee, C., Axson, J. L., Santander, M. V., and Prather, K. A.: Exploration of the effect of biological activity on the chemical mixing state of sea spray aerosols during a laboratory phytoplankton bloom, In Prep.

Tseng, R. S., Viechnicki, J. T., Skop, R. A., and Brown, J. W.: Sea-to-air transfer of surface-active organic compounds by bursting bubbles, Journal of Geophysical Research: Oceans (1978–2012), 97, 5201-5206, 10.1029/91JC00954, 1992.

Vaishya, A., Ovadnevaite, J., Bialek, J., Jennings, S. G., Ceburnis, D., and O'Dowd, C. D.: Bistable effect of organic enrichment on sea spray radiative properties, Geophysical Research Letters, 40, 6395-6398, 10.1002/2013GL058452, 2013.

Vesna, O., Sjogren, S., Weingartner, E., Samburova, V., Kalberer, M., Gäggeler, H., and Ammann, M.: Changes of fatty acid aerosol hygroscopicity induced by ozonolysis under humid conditions, Atmospheric Chemistry and Physics, 8, 4683-4690, 10.5194/acp-8-4683-2008, 2008.

Wang, X., Sultana, C. M., Trueblood, J., Hill, T. C. J., Malfatti, F., Lee, C., Laskina, O., Moore, K. A., Beall, C. M., McCluskey, C. S., Cornwell, G. C., Zhou, Y., Cox, J. L., Pendergraft, M. A., Santander, M. V., Bertram, T. H., Cappa, C. D., Azam, F., DeMott, P. J., Grassian, V. H., and Prather, K. A.: Microbial control of sea spray aerosol composition: A tale of two blooms, ACS Central Science, 1, 124-131, 10.1021/acscentsci.5b00148, 2015.

Wise, M. E., Surratt, J. D., Curtis, D. B., Shilling, J. E., and Tolbert, M. A.: Hygroscopic growth of ammonium sulfate/dicarboxylic acids, Journal of Geophysical Research: Atmospheres, 108, 10.1029/2003jd003775, 2003.

Zhang, X., Massoli, P., Quinn, P. K., Bates, T. S., and Cappa, C. D.: Hygroscopic growth of submicron and supermicron aerosols in the marine boundary layer, Journal of Geophysical Research: Atmospheres, 119, 8384-8399, 10.1002/2013JD021213, 2014.

Zhao, W. X., Hopke, P. K., and Prather, K. A.: Comparison of two cluster analysis methods using single particle mass spectra, Atmospheric Environment, 42, 881-892, 10.1016/j.atmosenv.2007.10.024, 2008.

Table 1. Summary of all instrumentation used in this study.

Sampling Group	Group MART Flow Rates (LPM) Input/Output	Group Sampling Duration (hours)	Group Sampling Time After Group #1 (hrs)	Instrument/Method	Property Measured	Reference
			Particle Measurements			
1	4.7 /3.7	1.5	0	UCD Cavity Ringdown Spectrometer (CRD)	Light extinction by dry (<20% RH) and humidified (RH ~85%) particles	(Langridge et al., 2011; Cappa et al., 2012)
1	4.7 /3.7	1.5	0	Scanning Electrical Mobility Analyzer (SEMS)	Dry particle mobility size distributions from $d_{p,m}$ = 15 to 1000 nm	
1	4.7/3.7	1.5	0	High Resolution Time of Flight Aerosol Mass Spectrometer (HR-ToF-AMS)	Bulk concentrations of non-refractory particulate components of dry particles from d_{va} = 90 nm to 700 nm	(Canagaratna et al., 2007)
2	3.9/2.9	2.0	9	Aerosol Time of Flight Mass Spectrometer (ATOFMS)	Composition and number concentration of dried individual particles from d_{va} = 300 nm to 3000 nm	(Gard et al., 1998; Pratt et al., 2009)
3	6.3/5.3	1.0	4.5	Aerodynamic Particle Sizer (APS)	Dry particle aerodynamic size distributions (0.7-20 μm)	
			Waterside Measurements			
				Aquaflour handheld portable fluorimeter	Chlorophyll-a	
				High temperature combustion	Dissolved organic carbon	
				Epifluorescence microscopy	Heterotrophic bacteria concentrations	

Table 2. Seawater conditions at the time of collection

Date	Time	Chlorophyll-a (ug/L)	Water Temp. (°C)	Pressure (dbar)	Salinity (PSU)
8 July	12:00	0.998	23.1214	3.389	33.546
19 July	12:00	2.171	20.7463	3.567	33.6051

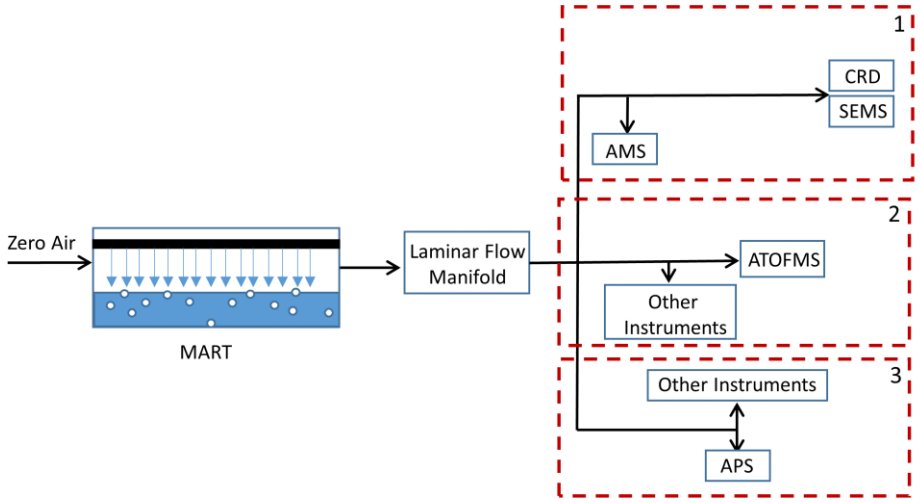

Figure 1. Experimental schematic for MART sampling during the IMPACTS 2014 study, with boxes labeled 1, 2, and 3 corresponding to different sampling configurations.

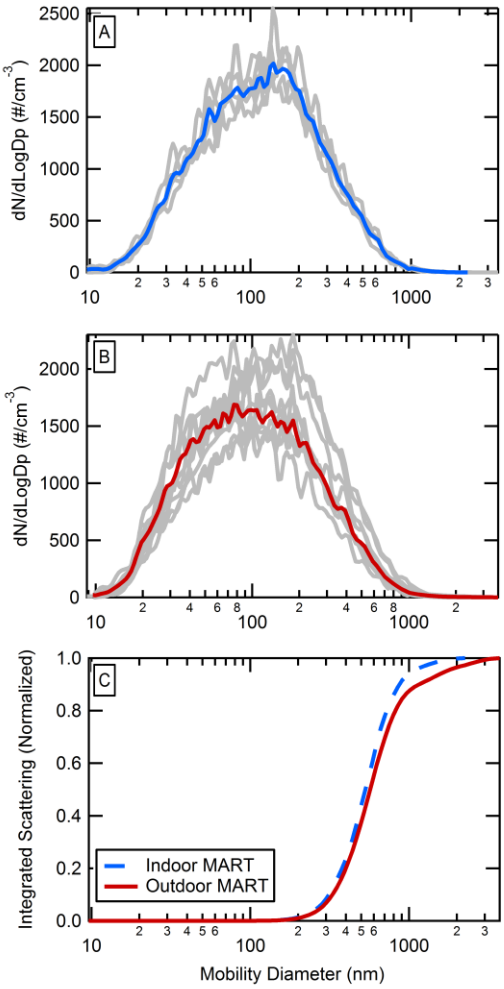

Figure 2. Single (grey) and average (red or blue) number-weighted merged size distributions for the **(A)** "indoor" and **(B)** "outdoor" MARTs averaged over the MART sampling period (1.5 hours) and **(C)** normalized integrated scattering as a function of dry mobility diameter for the merged size distribution. The optically-weighted median diameters are 530 nm for the indoor MART and 570 nm for the outdoor MART.

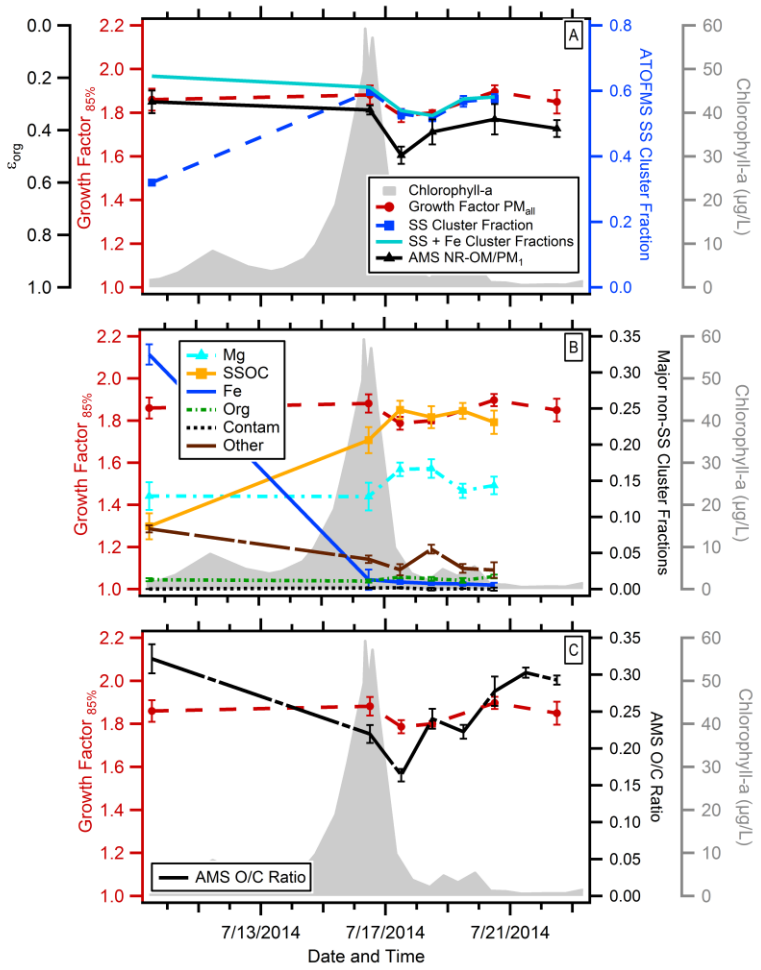

Figure 3. Time series for the indoor MART chlorophyll-a (gray), PM_{all} *GF*(85%) (red circles), and **(A)** organic volume fraction (ε_{org}) estimated from AMS non-refractory organic matter (NR-POM)/ PM_1 mass (solid black line), ATOFMS sea salt (SS) cluster fractions (blue dashed line), and ATOFMS SS + Iron type (Fe) cluster fractions **(B)** dominant non-sea salt cluster fractions magnesium (Mg) type (dashed turquoise line), Fe, "Other" type, and contamination (black line) and sea salt with organic carbon (SSOC) (orange line) cluster fractions, and **(C)** the AMS O/C ratio (dashed black line). Note that the axis for ε_i is reversed to facilitate comparison to *GF*(85%) values. The reported standard deviations for all properties is 1σ of the individual measurements over each sampling period.

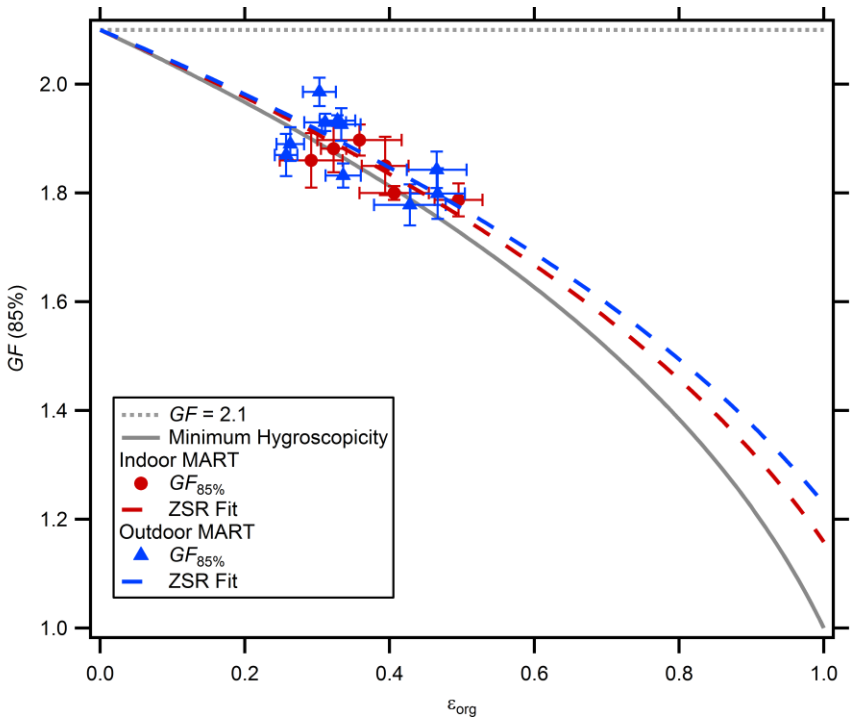

Figure 4. PM_{all} *GF*(85%) as a function of the fraction of organic volume fraction estimated from AMS non-refractory organic matter (NR-POM)/ PM_1 mass for the indoor (red circles) and the outdoor (blue triangles) MARTs. ZSR fits to the data using Equation 5 are shown for the indoor (dashed red line) and outdoor (dashed blue line) MARTs, assuming $GF_{sea\ salt}(85\%) = 2.1$ (dotted grey line). The overall retrieved $GF_{org}(85\%)$ values were 1.16 ± 0.09 and 1.23 ±0.10 for the indoor and outdoor MARTs, respectively. The grey solid line connecting *GF*(85%) = 2.1 and $GF_{org}(85\%) = 1.0$ provides the minimum value expected for any combination of *GF*(85%) .

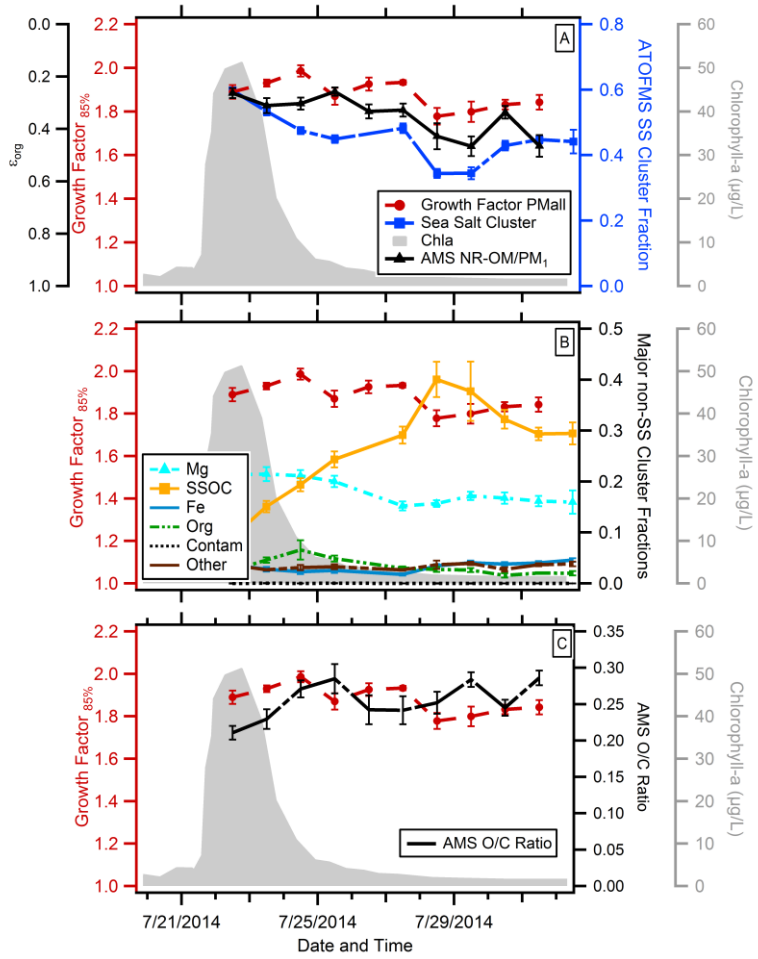

Figure 5. Same as Figure 3 above, but for the outdoor MART.

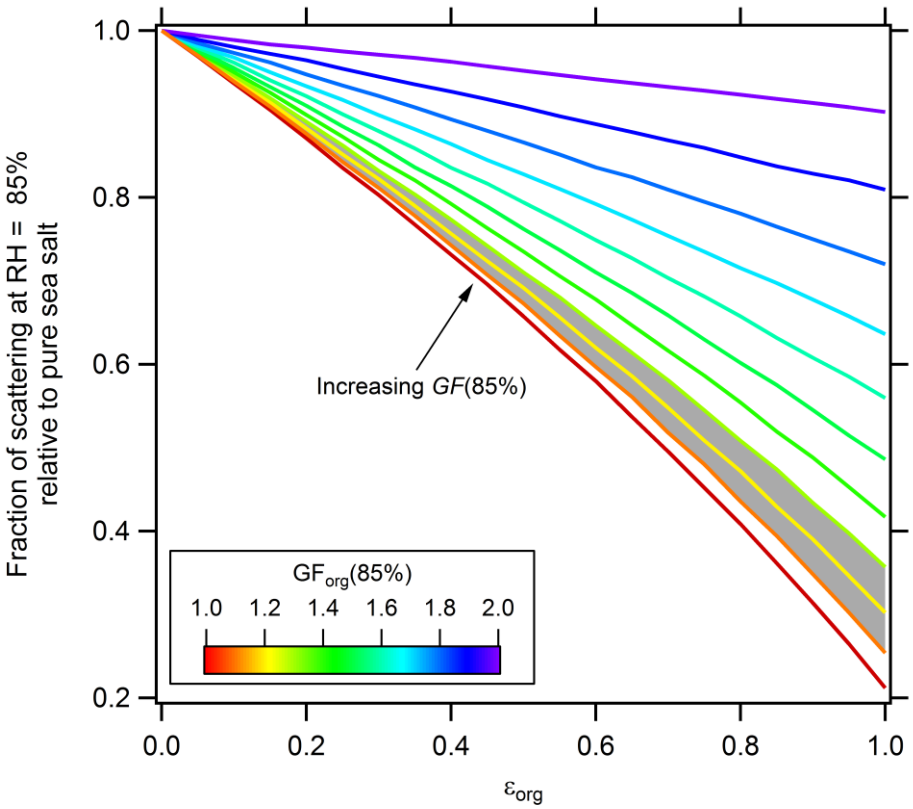

Figure 6. Calculated fraction of scattering relative to pure sea salt particles at 85% RH as a function of ε_{org}, assuming the OM component of the SSA particles have the same, constant hygroscopicity and a refractive index of 1.55 and the SSA particles follow the ZSR mixing rules. The different curves are colored according to the assumed $GF_{org}(85\%)$ value, ranging from 1.0 to 2.0, given $GF_{sea\ salt}(85\%) = 2.1$. The gray band shows the range of GF_{org} values indicated by the current measurements.

Supplementary Online Material for "Linking variations in sea spray aerosol particle hygroscopicity to composition during two microcosm experiments"

Sara D. Forestieri[1], *Gavin C. Cornwell*[2], *Taylor M. Helgestad*[1], *Kathryn A. Moore*[2], *Christopher Lee*[2], *Gordon A. Novak*[3], *Camille M. Sultana*[2], *Xiaofei Wang*[2], *Timothy H. Bertram*[2,3], *Kimberly A. Prather*[2,4], *Christopher D. Cappa*[1,*]

[1]Department of Civil and Environmental Engineering, University of California, Davis, CA 95616

[2] Department of Chemistry and Biochemistry, University of California, San Diego, La Jolla, CA 92093

[3] Department of Chemistry, University of Wisconsin, Madison, WI 53706

[4] Scripps Institution of Oceanography, 9500 Gilman Drive, La Jolla, CA 92093

[*] Correspondence to: E-mail: cdcappa@ucdavis.edu

The supplementary material consists of six figures that provide additional support for the conclusions presented in the paper.

Table S1. Summary of uncertainties for growth factor (GF) retrieval.

Parameter	Default Value	Perturbation	ΔGF	% ΔGF
f(RH)	3.7	0.5 (7%)[#]	0.05	2.6%
Relative Humidity	85%	1.2%/0.03% (see Table 2)	0.05/0.01[$]	2.4%/0.5%
Refractive Index	1.55	0.04	0.05	2.7%
Particle Diameter	Distribution with mode = ~112 nm	+1%	0.01	<1%

[$] ΔGF values were calculated using Kappa-Kohler equation and assuming a κ value of 1.3 [*Petters and Kreidenweis*, 2007].

Table S2. Measured and actual GFs for pure substances and the implied error in the measured RH.

	Observed	Actual	ΔRH
NaCl	2.09	2.1	0.03%
Ammonium Sulfate	1.59	1.55	1.2%

Uncertainties in the measured f(RH), relative humidity, refractive index, and diameter that contribute to the overall uncertainty in GF retrieval are provided in Table S1. The uncertainty in the CRD extinction is ~5% at 532 nm and the fundamental performance of the CRD method for wet particles is not changed. Therefore, the propagated uncertainty of f(RH) (=$bext_{wet}/bext_{dry}$) = $\sqrt{0.05^2 + 0.05^2}$ = 7%. Two estimates for uncertainty in relative humidity were based on the hygroscopic growth factors of pure NaCl and pure ammonium sulfate generated from a TSI atomizer. The measured values were compared to literature values to infer the error in RH (see Table 2). The refractive index used in this study is appropriate for NaCl. However, refractive index of sea salt mixed with marine derived organic matter is not well known, but a value of 1.48 reported by Nessler et al. [2005] for organic matter has been used in many recent studies [*Partanen et al.*, 2014; *Vaishya et al.*, 2013] for marine derived organic matter. The refractive index of the mixture

is likely to be somewhere in between. Assuming that organic matter is 50% of the particles by volume (consistent with the ensemble average fraction reported in this manuscript), the volume-weighted refractive index is 1.51. GF values were retrieved with a refractive index of 1.51 and compared to the GF values retrieved using the default value of 1.55 to assess the uncertainty in the refractive index. The uncertainty of 1% for the measured diameter was determined during the experiments in which a 2nd DMA size-selected particles 100-300 nm.

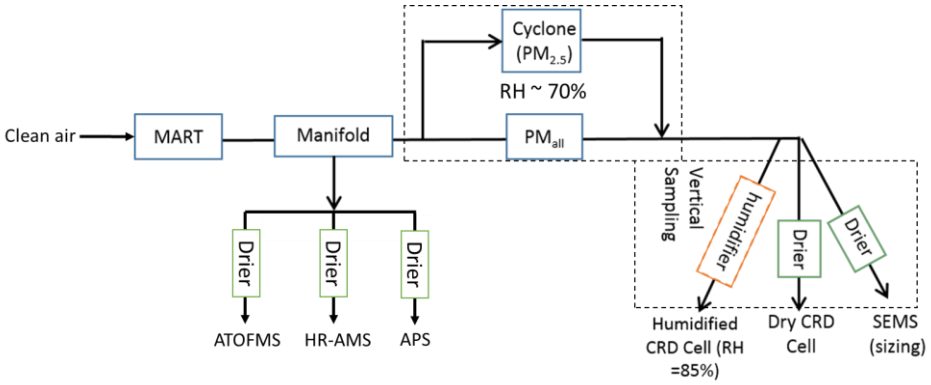

Figure S1. A detailed schematic of the general sampling scheme for the online instruments. Note that not all instruments sampled at the same time (see Table 1). Particles sampled from the MART passed through a manifold from which they were subsampled to the various instrumentation. All instruments included an upstream drier and sampled dried particles. The driers and humidifiers for the CRD and SEMS sampling group (Group 1) were oriented vertically. The particles sampled to the CRD and SEMS alternately passed through a $PM_{2.5}$ cyclone. The RH at this point was ~70%.

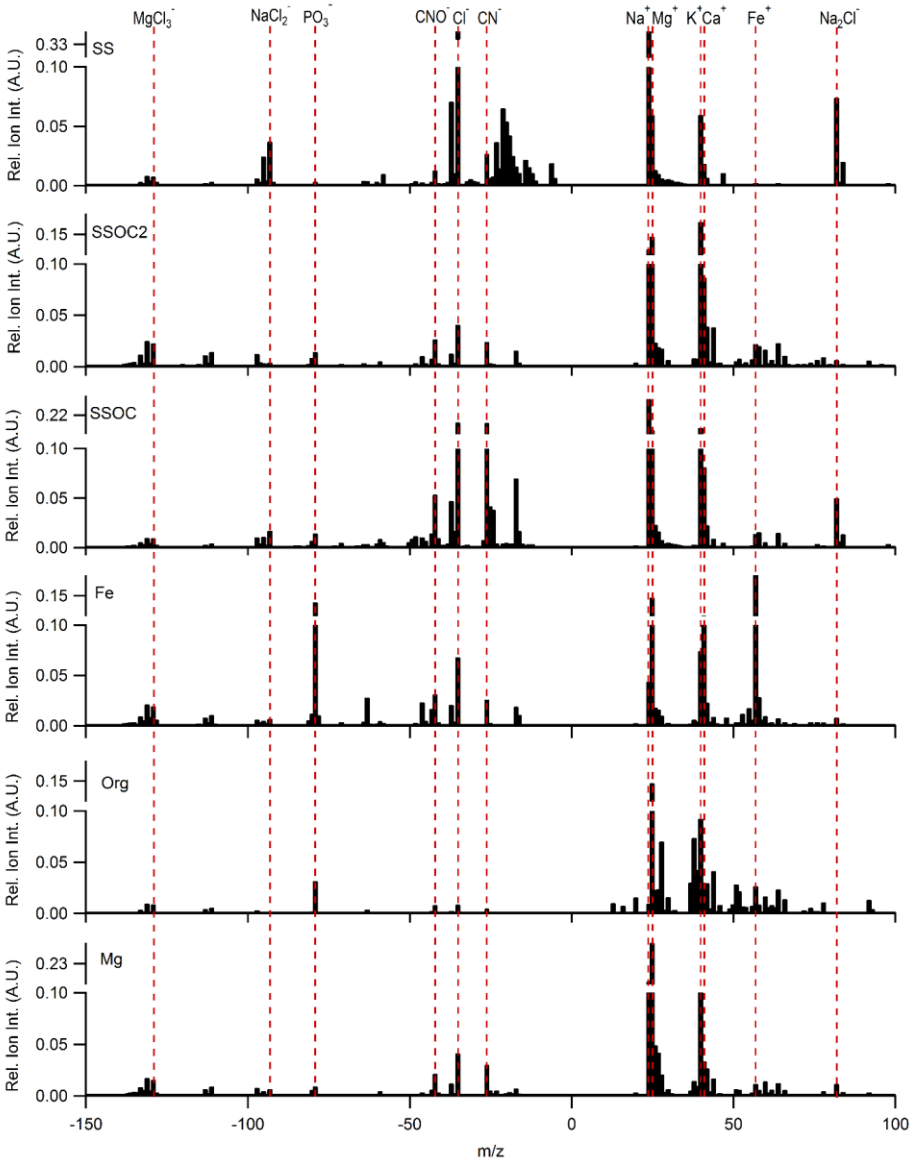

Figure S2. Dual polarity ATOFMS Mass Spectra for the major spectra categories: sea salt (SS), sea salt with organic carbon (SSOC and SSOC2), Iron (Fe), Organic (Org), and Magnesium (Mg) types.

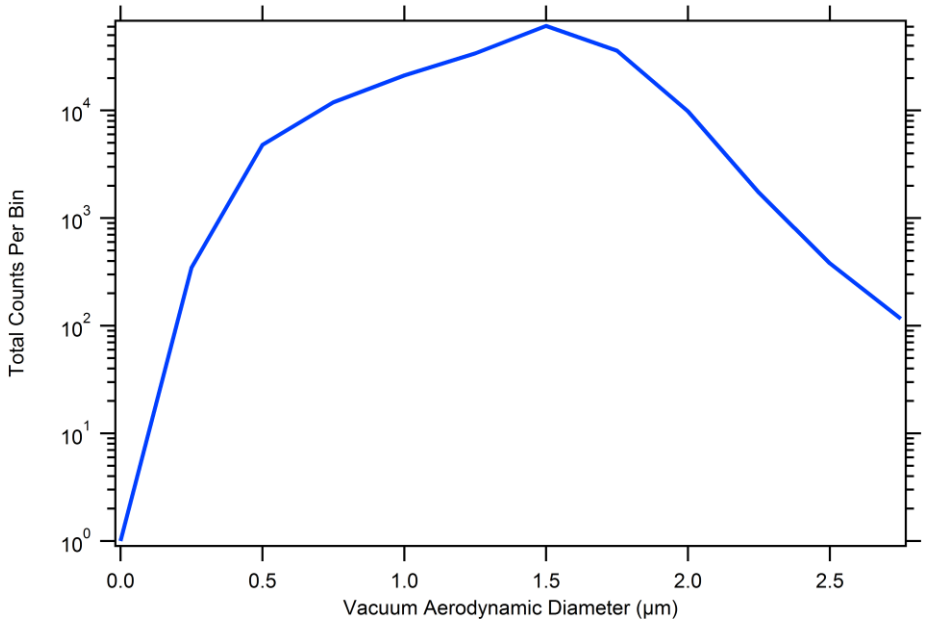

Figure S3. Size-resolved ATOFMS particle counts.

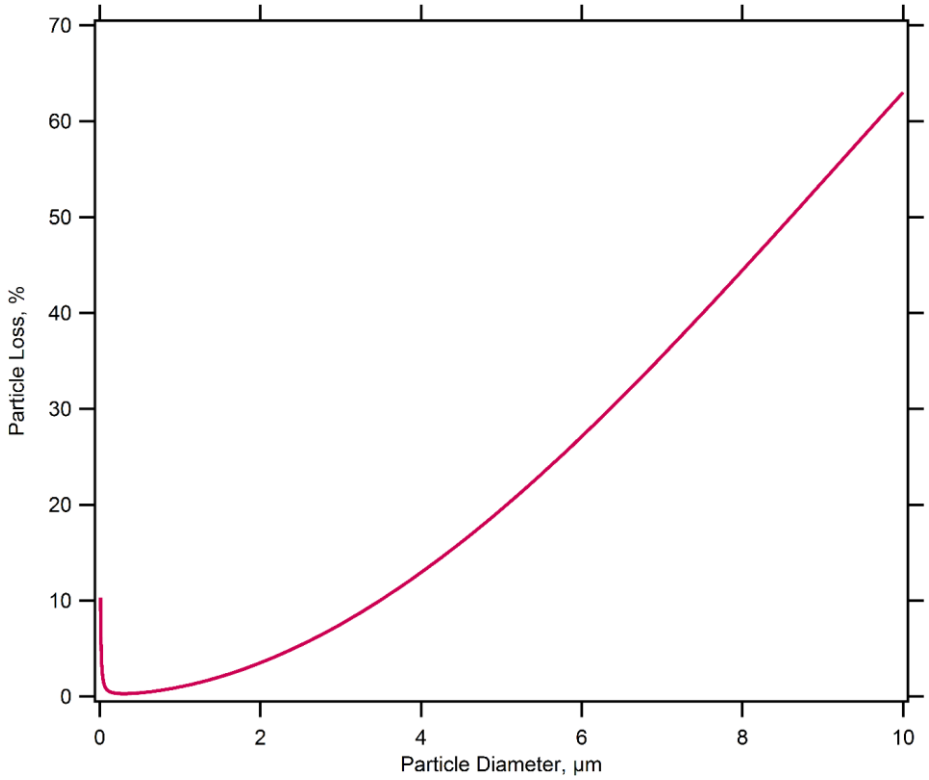

Figure S4. Predicted particle losses for particles travelling from the MART outlet to the MART manifold for a sampling line 10' in length and 3/8" in diameter. The Particle Loss Calculator of [*Von der Weiden et al.*, 2009] was used.

Formatted: Font color: Accent 1

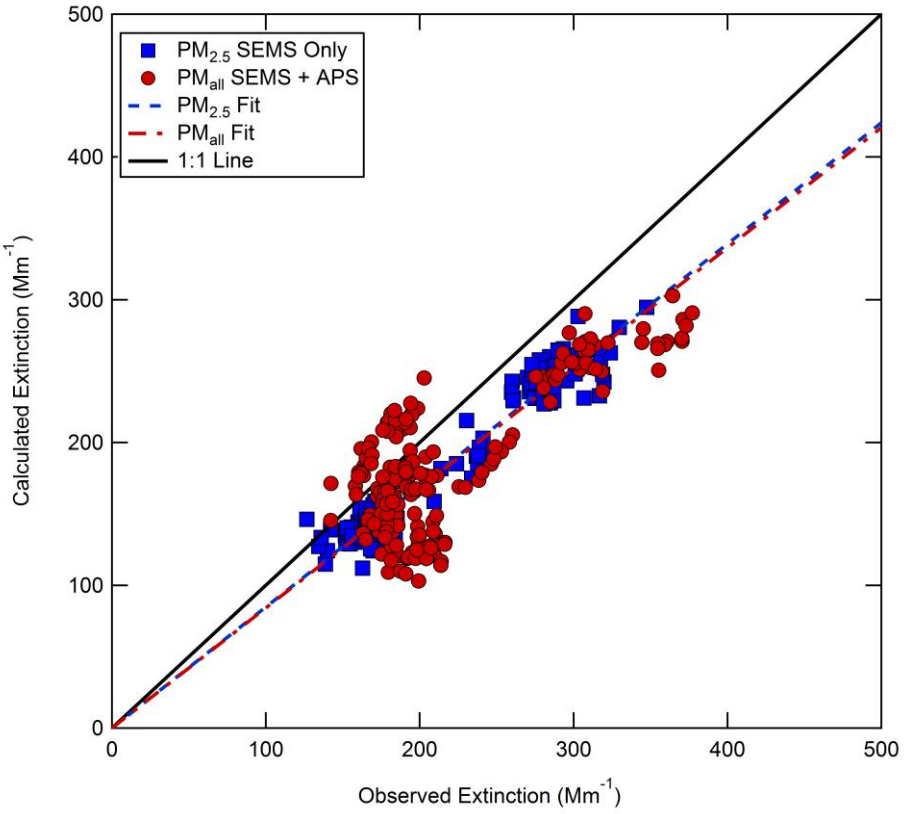

Figure S5. Calculated extinction using SEMS size distributions (real RI = 1.55) for $PM_{2.5}$ and SEMS+APS size distributions as a function of the observed CRD extinction for the 2014 MART experiments. Slopes for linear fits (with the intercept fixed at 0) of calculated extinction as a function of observed extinction were 0.85 and 0.84 for $PM_{2.5}$ and PM_{all}, respectively. A 1:1 line is provided for reference.

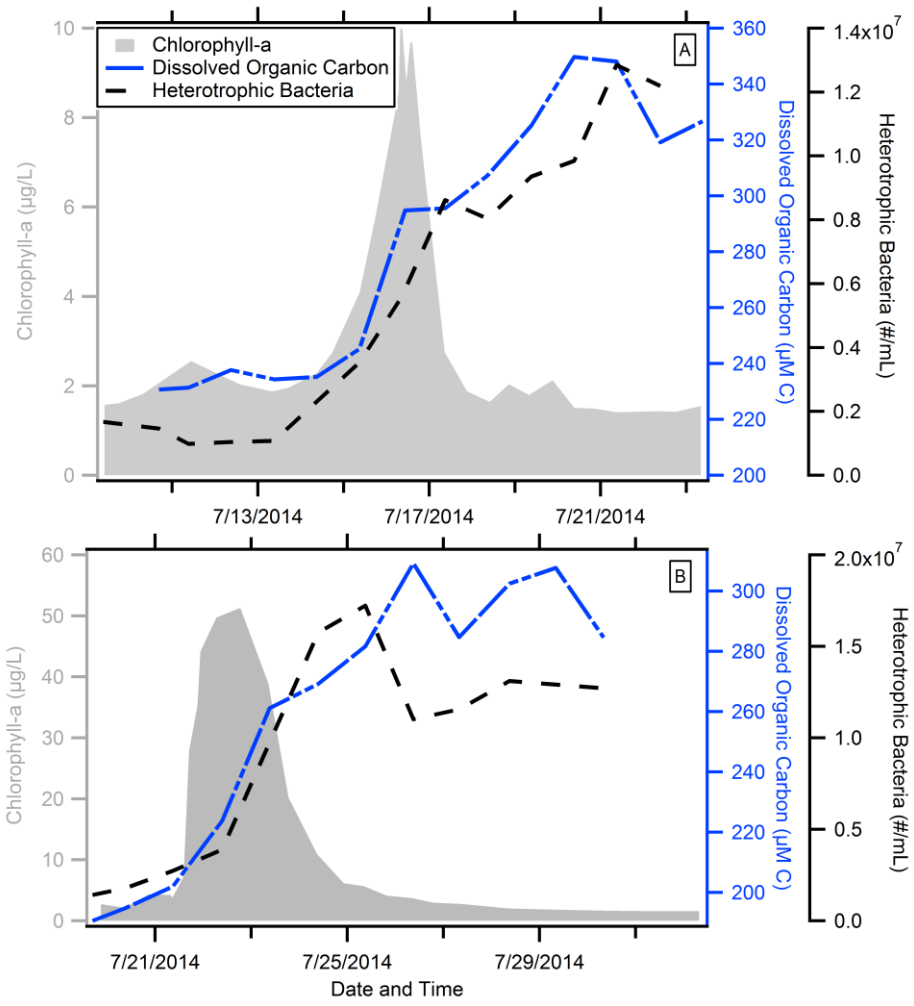

Figure S6. Time series of concentrations of dissolved organic carbon (DOC; µM C), heterotrophic bacteria (#/mL), and chlorophyll-a concentrations (µg/L) in the seawater water for the (A) indoor and (B) outdoor MARTs.

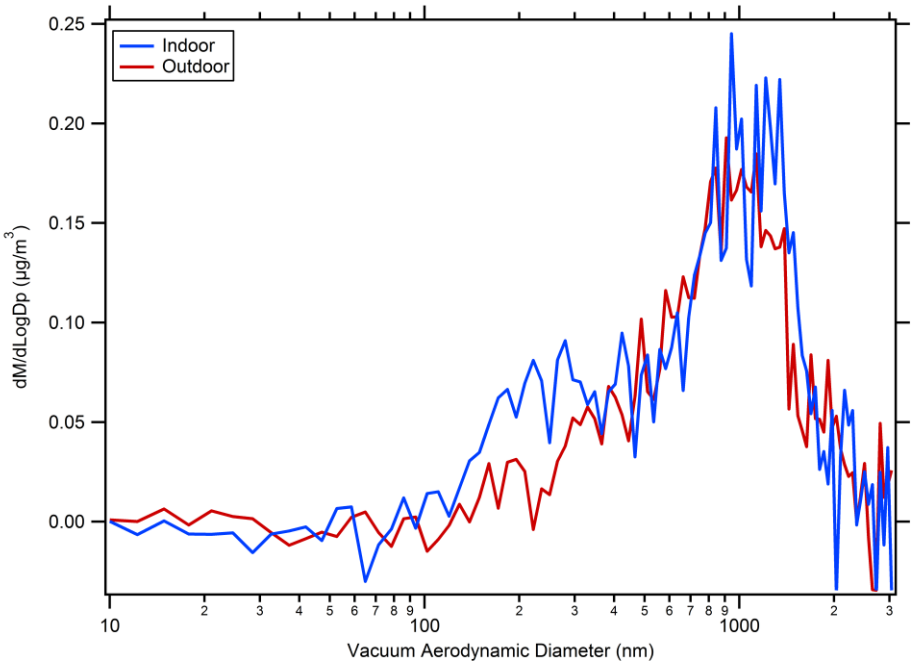

Figure S7. AMS m/z 43 particle time of flight (pTOF) mass distributions for the indoor (blue) and outdoor (red) MARTS.

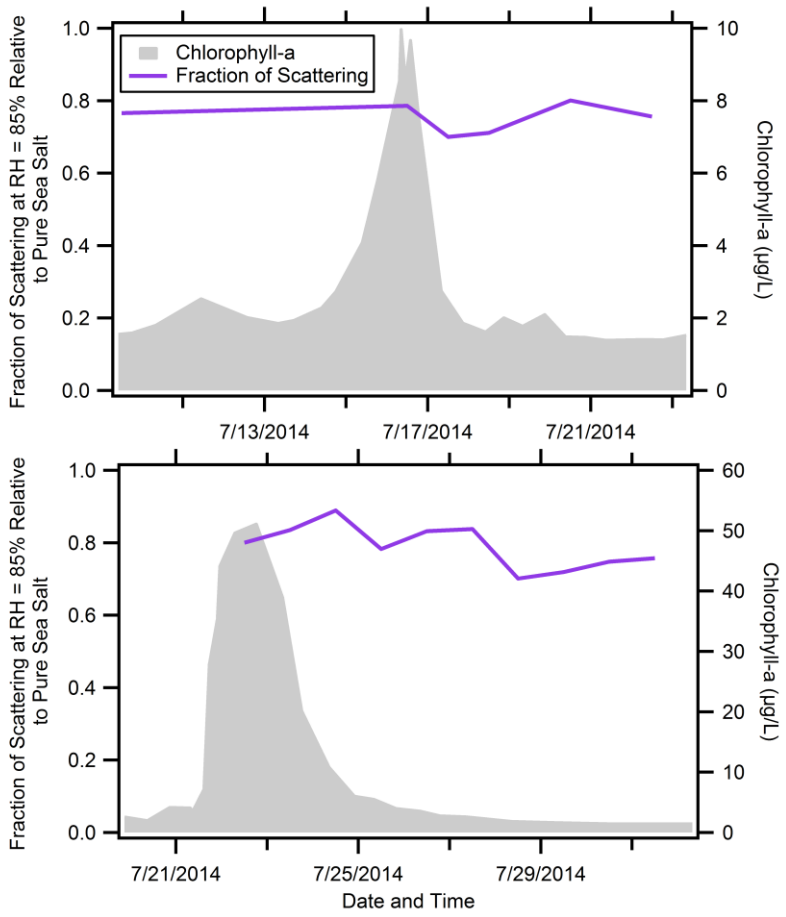

Figure S8. Calculated fraction of scattering relative to pure sea salt particles at 85% RH as a function of time for the two microcosm experiments.

References

DeCarlo, P. F., J. G. Slowik, D. R. Worsnop, P. Davidovits, and J. L. Jimenez (2004), Particle morphology and density characterization by combined mobility and aerodynamic diameter measurements. Part 1: Theory, *Aerosol Science and Technology*, *38*(12), 1185-1205.

Nessler, R., E. Weingartner, and U. Baltensperger (2005), Adaptation of dry nephelometer measurements to ambient conditions at the Jungfraujoch, *Environmental science & technology*, *39*(7), 2219-2228.

Partanen, A. I., et al. (2014), Global modelling of direct and indirect effects of sea spray aerosol using a source function encapsulating wave state, *Atmospheric Chemistry and Physics*, *14*(21), 11731-11752.

Petters, M., and S. Kreidenweis (2007), A single parameter representation of hygroscopic growth and cloud condensation nucleus activity, *Atmospheric Chemistry and Physics*, *7*, 1961-1971.

Vaishya, A., J. Ovadnevaite, J. Bialek, S. G. Jennings, D. Ceburnis, and C. D. O'Dowd (2013), Bistable effect of organic enrichment on sea spray radiative properties, *Geophysical Research Letters*, *40*(24), 6395-6398.

Von der Weiden, S., F. Drewnick, and S. Borrmann (2009), Particle Loss Calculator–a new software tool for the assessment of the performance of aerosol inlet systems, *Atmos. Meas. Tech*, *2*(2), 479-494.